This article has been accepted for publication in Monthly Notices of the Royal Astronomical Society Published by Oxford University Press.

https://doi.org/10.1093/mnras/stad3878

Swift/XRT observations of superorbital modulations in wind-fed supergiant X-ray binaries

P. Romano,[1★] E. Bozzo,[2,3] N. Islam,[4,5] R.H.D. Corbet,[6,5,7]

[1]*INAF, Osservatorio Astronomico di Brera, Via E. Bianchi 46, I-23807, Merate, Italy*
[2]*Department of Astronomy, University of Geneva, Chemin d'Ecogia 16, CH-1290 Versoix, Switzerland*
[3]*INAF-OAR, Via Frascati, 33, 00078 Monte Porzio Catone, Rome, Italy*
[4]*Center for Space Science and Technology, University of Maryland, Baltimore County, 1000 Hilltop Circle, Baltimore, MD 21250, USA*
[5]*X-ray Astrophysics Laboratory, NASA Goddard Space Flight Center, Greenbelt, MD 20771, USA*
[6]*CRESST and CSST, University of Maryland, Baltimore County, 1000 Hilltop Circle, Baltimore, MD 21250, USA*
[7]*Maryland Institute College of Art, 1300 W Mt Royal Ave, Baltimore, MD 21217, USA*

ABSTRACT

We present the first *Swift*/XRT long-term monitoring of 2S 0114+650, a wind-fed supergiant X-ray binary for which both orbital and superorbital periods are known (P_{orb} ~11.6 d and P_{sup} ~30.8 d). Our campaign, summing up to ~ 79 ks, is the most intense and complete sampling of the X-ray light curve of this source with a sensitive pointed X-ray instrument, and covers 17 orbital, and 6 superorbital cycles. The combination of flexibility, sensitivity, and soft X-ray coverage of XRT allowed us to confirm previously reported spectral changes along the orbital cycle of the source and unveil the variability in its spectral parameters as a function of the superorbital phase. For completeness, we also report on a similar analysis carried out by exploiting XRT archival data on three additional wind-fed supergiant X-ray binaries IGR J16418−4532, IGR J16479−4514, and IGR J16493−4348. For these sources, the archival data provided coverage along several superorbital cycles but our analysis could not reveal any significant spectral variability.

Key words: accretion: accretion discs; X-rays: stars; X-rays: binaries; stars: neutron; stars: massive; X-rays: individual: 2S 0114+650; X-rays: individual: IGR J16418−4532; X-rays: individual: IGR J16479−4514; X-rays: individual: IGR J16493−4348.

1 INTRODUCTION

Superorbital modulations have been detected in the past decade from several different classes of X-ray binaries, containing both neutron star (NS) and black hole accretors. These modulations are revealed by exploiting long-term (typically months to years) monitoring observations of relatively bright systems in the X-rays and usually appear as significant peaks in the system power density spectra with periodicities that can be as long as several to tens of times those associated with the binary orbital period (see, e.g., Sood et al. 2007, for a historical review). In those X-ray binaries where the accretion takes place via an accretion disk around the compact object, the superorbital modulation is commonly ascribed to the precession of a (sometimes) warped disk. The precession model has been extensively applied to systems like Her X-1, where spectroscopic investigations in the X-ray domain were able to constrain in fairly good detail the geometry of the X-ray emission along an entire superorbital cycle (see, e.g., Brumback et al. 2021, and references therein). The precessing accretion disk model has also been able to convincingly explain the superorbital modulations observed from LMC X-4 (Ambrosi et al. 2022) and SMC X-1 (Brumback et al. 2020; Pradhan et al. 2020).

It proved considerably more complicated to explain the superorbital modulations revealed from wind-fed X-ray binaries, where the accretion onto the compact object takes place directly from the strong wind of a massive companion (without the presence of a disk). Wind-accreting X-ray binaries are generally fainter than disk-fed systems and thus revealing superorbital modulations requires years of monitoring observations carried out with large field-of-view (FOV) instruments (e.g., those on-board *RXTE*, *INTEGRAL*, and *Swift*; see Corbet & Krimm 2013, for a recent review). In this class of sources, alternative models for the superorbital modulations have been proposed. Koenigsberger et al. (2003) and Moreno et al. (2005) showed that oscillations induced in non-synchronously rotating stars in binary systems could lead to changes in the mass loss rates (and thus on the accretion-driven X-ray luminosity) on periods longer than the binary orbital period. Alternatively, the presence of a third body in a more distant orbit but gravitationally bound to the binary could also produce a periodic long-term variation of the X-ray luminosity (see, e.g. Farrell et al. 2008, and references therein). More recently, Bozzo et al. (2017) proposed that the superorbital modulation could be associated with the periodic interaction between the accreting compact object and the so-called corotating interaction regions (CIRs) around the massive companion. These structures are known to extend for several stellar radii around OB supergiants, be-

★ E-mail: patrizia.romano@inaf.it

ing characterized by a substantial over-density compared to the surrounding stellar wind and a possibly asynchronous velocity with respect to the massive star rotation. Due to their physical properties, the interaction between the NS and the CIRs is expected to lead not only to an X-ray intensity variation but also to changes (by a factor of a few) of the absorption column density local to the source (see also Lobel & Blomme 2008, and references therein).

Currently, only six wind-fed binaries are known to show superorbital modulations, IGR J16479−4514, IGR J16418−4532, 2S 0114+650, 4U 1538−522, 4U 1909+07, and IGR J16493−4348. All of them displayed a puzzling virtually identical ratio between the orbital and superorbital periodicity of a factor of 2.7–4 (Corbet & Krimm 2013; Coley et al. 2019; Corbet et al. 2021; Islam et al. 2023). Attempts have been made in the literature to interpret their superorbital modulations in the context of the three models described above. Corbet & Krimm (2013) argued that the applicability of the stellar oscillations and the third body model are rather difficult. The former scenario requires circular orbits (see also Moreno et al. 2011) and it is hardly compatible with the high coherency of the superorbital modulations. The second scenario could be compatible with the high coherency but the measured virtually constant ratio between the orbital and superorbital periodicity of a factor of ∼2.7–4 across different sources would require unrealistic constraints on their formation conditions (especially in view of the expectation that these should eventually be hierarchical systems hosting a distant third body). Corbet et al. (2021) and Islam et al. (2023) discussed how the CIR model could provide a more likely explanation for most sources, with the virtually constant ratio between the system orbital and superorbital modulations associated with a pseudo-synchronization of the CIR rotational period with the NS orbit.

Investigations of the origin of the superorbital modulations in wind-fed X-ray binaries in the X-ray domain have so far relied on two kinds of observational campaigns: (i) long term monitoring provided (mostly) at hard X-rays by large FOV instruments, and (ii) relatively short (few tens of ks) pointed observations per object during a specific superorbital phase. Monitoring observations proved so far crucial to discover the periodicities, although they generally provide limited information on possible spectral variations along the superorbital cycle due to the relatively low sensitivity and signal-to-noise ratio (S/N) over short time scales (see, e.g., Corbet & Krimm 2013; Corbet et al. 2017, and references therein). Pointed observations carried out also with multiple facilities at the same time are characterized by a much higher sensitivity and allow in-depth analysis of the intensity and spectral energy distribution of the source. However, they are affected by the limitation of providing only a snapshot of the binary system during a relatively short time interval and it is thus difficult to unambiguously link any measured variability of the source intensity or of any identified spectral feature with the superorbital phase. As discussed by Bozzo et al. (2017), wind-fed binaries are commonly characterized by a prominent intensity and spectral variability (on time scales of hundreds of seconds to hours) due to the clumpiness of the stellar wind (see also Martínez-Núñez et al. 2017; Kretschmar et al. 2019, for recent reviews) from the companion star. A proper study of any source variability with the superorbital phase thus requires long-term observations carried out across many cycles with high sensitivity, so that they can be folded over the superorbital period and ensure the short-term variability due to the stellar wind clumps is averaged out.

In the past, the process of averaging X-ray observations has been exploited to unveil the presence of long-lived structures surrounding the accreting compact objects in wind-fed X-ray binaries along their orbital rather then their superorbital cycles. For very bright X-ray sources as Vela X-1, GX 301-2, and 4U 1538-52, the data collected by the Monitor of All Sky X-ray Image (Matsuoka et al. 2009, MAXI) proved particularly interesting due to their extended energy coverage over many orbital revolutions since the beginning of the experiment scientific operations back in 2009 (Doroshenko et al. 2013; Islam & Paul 2014; Rodes-Roca et al. 2015). However, the vast majority of the wind-fed X-ray binaries are either too faint or located into crowded sky regions to be efficiently accessed by the MAXI capabilities. For all these cases, our group has extensively demonstrated that observations with the narrow-field instrument, the X–ray Telescope (XRT, Burrows et al. 2005) on-board the Neil Gehrels *Swift* Observatory (Gehrels et al. 2004), are very well suited (Ferrigno et al. 2022).

In this paper, we present for the first time the exploitation of XRT data to probe spectral variability not only on the orbital but also along the superorbital cycles of wind-fed X-ray binaries. In particular, we report on the outcomes of a new long-term XRT observational campaign focused on 2S 0114+650. The campaign was specifically designed to unveil spectral and intensity variability of this wind-fed binary along its superorbital cycle. Thanks to the regular monitoring and the enhanced sensitivity of *Swift*/XRT, we can now simultaneously average data over multiple orbital and superorbital cycles, a crucial step in mitigating short-term X-ray intensity variations and exploring long-term spectral changes. We also report the results obtained by applying the same techniques as those exploited in the case of 2S 0114+650 on archival data collected from three further wind-fed binaries, IGR J16418-4532, IGR J16479-4514, and IGR J16493-4348 (see Table 1). For these objects the past observational campaigns, albeit not optimized for the search of variability associated to the superorbital period, contained sufficient data to apply our method. A brief summary of the current knowledge on all sources we considered is given in Sect. 2. In Sect. 3, we provide a description of the *Swift*/XRT data (with log tables included in Appendix A) and the data-reduction technique. An overview of the results we obtained and their discussion are provided in Sect. 4.

Table 1. Properties of the sources studied in this paper.

Source	P_{orb} (d)	P_{sup} (d)	T_0[a] (MJD)	References P_{orb}	References P_{sup}
2S 0114+650	11.5983±0.0006[b]	30.76±0.03	53488	1	2
IGR J16418−4532	3.73886±0.00003	14.730±0.006	55994.6	3	2
IGR J16479−4514	3.3193±0.0005	11.880±0.002	55996	4	2
IGR J16493−4348	6.782±0.005	20.07±0.01	54265.1	5	2,6

References: (1) Grundstrom et al. (2007); (2) Corbet & Krimm (2013); (3) Levine et al. (2011); (4) Romano et al. (2009); (5) Cusumano et al. (2010); (6) Coley et al. (2015).

Notes: [a] Phase zero for the superorbital period is the minimum of the folded light curve for 2S 0114+650 Farrell et al. (2008), the maximum for the remainder of the sample. [b] Phase zero for the orbital period is the time of periastron passage from Grundstrom et al. (2007) at MJD 51824.8.

2 THE SOURCE SAMPLE

In the sub-sections below, we briefly describe the current knowledge on all sources considered in this paper. We focus more on 2S 0114+650, which is the target of our recent observational campaign with *Swift*/XRT. The other three sources (IGR J16418-4532, IGR J16479-4514, and IGR J16493-4348) are briefly mentioned for completeness, as we apply to their archival data (already analyzed in previous work) the same analysis techniques used in the case of 2S 0114+650.

2.1 2S 0114+650

2S 0114+650 was discovered in 1977 and readily classified as a supergiant high-mass X-ray binary, with the companion star being identified as a B1Ia supergiant (LS I+65 010) at a distance of ~7.2 kpc (SgXB; Dower et al. 1977; Reig et al. 1996). The nature of the accretor was confirmed as a NS with the discovery of a 2.73 h spin period (see, e.g. Hall et al. 2000, and references therein). Subsequent measurements of the source spin period also led to the discovery and monitoring of spin-up and spin-down phases (Falanga et al. 2015). The measured orbital period of the system is ~11.6 d, while the estimated eccentricity is ~0.18 (Koenigsberger et al. 2006).

The profile of the X-ray variability along the binary orbit shows the typical modulation expected for a wind-fed system (Grundstrom et al. 2007) but it is also characterized by a peculiar stable dip at the inferior conjunction which is most likely associated with a localized increase in the absorption column density rather than an X-ray eclipse (see Pradhan et al. 2015, and references therein).

S 0114+650 also exhibits a 30.76 d superorbital modulation of its X-ray emission, which origin has long been investigated but still remains unclear (Farrell et al. 2006; Corbet & Krimm 2013). Hu et al. (2017) performed a detailed study of the long-term evolution of the spin, orbital, and superorbital modulations of the source by using *Swift*/BAT and *RXTE*/ASM data. These authors found that the NS spin period undergoes both episodes of intense and prolonged spin-up/spin-down, and episodes of more irregular and moderate variations. The orbital and superorbital periodicities were found to be stable over time, although the intensities of these modulations can vary substantially and generally the superorbital one decreases during times when the NS spin period variations are more erratic. Hu et al. (2017) suggested that a temporary accretion disk could form around the NS in 2S 0114+650, such that the source switches periodically from wind to disk accretion. During the disk accreting periods, the spin-up/spin-down is stronger and more regular, while during wind accretion it turns into a more complex behavior, as expected due to the clumpiness of the stellar wind affecting the accretion. The weakening of the superorbital modulation intensity is more pronounced during the time intervals when the source is suspected to switch to the wind accretion. The authors thus advanced the hypothesis that the modulation itself could be somehow closely linked to the presence of an accretion disk.

The broad-band X-ray spectrum of 2S 0114+650 has been measured several times in the past decades using different facilities. The source spectral energy distribution is closely reminiscent of what is usually observed from wind-fed systems and well described by a model comprising a substantially absorbed (3–5×10^{22} cm^{-2}) cut-off power law. The cut-off energy is found to be in the range 10–30 keV, while typical power-law photon indices vary between 1.0–2.3 (Farrell et al. 2008; Pradhan et al. 2015; Abdallah et al. 2023). To the best of our knowledge, a detailed study of the spectral variability of the source along its orbital and superorbital cycles have been presented in the past only by Farrell et al. (2008). These authors used an absorbed cut-off model to describe the source X-ray emission measured by the *RXTE*/PCA and revealed a modest change in both the source absorption column density and photon index as a function of the orbital phase. In particular, they found that the spectrum is harder and less absorbed when the source emission is fainter. A similar trend for the photon index and absorption column density was suggested for the superorbital case as well, although the error bars associated with the measurements were far too large to draw any firm conclusion. No changes were measured as a function of both the orbital and superorbital period for the cut-off energy.

2.2 The other sources: IGR J16418-4532, IGR J16479-4514, and IGR J16493-4348

IGR J16418-4532 has been classified as an intermediate supergiant fast X-ray transient (SFXTs; e.g. for recent reviews, see Walter et al. 2015; Martínez-Núñez et al. 2017) since flares from this source have been observed several times (Tomsick et al. 2004; Sguera et al. 2006; Ducci et al. 2010; Romano et al. 2012a; Krimm et al. 2013; Romano et al. 2014, 2023) but the overall dynamic range in the X-ray luminosity remains as of today limited to values somewhat smaller than those typical of the bulk of the SFXT population (Romano et al. 2015). The source displays clear eclipses, with a measured orbital period of 3.73 days. The nature of the compact object has been firmly established to be a NS thanks to the discovery of X-ray pulsations with a period of ~1210 s (Sidoli et al. 2012). A precise classification of the donor star is still missing, given the fact that different authors have discussed both the possibility of an O or B supergiant located at about 13 kpc (Coleiro et al. 2013; Coley et al. 2015). IGR J16418-4532 is also known to typically display a large absorption column density, exceeding 10^{23} cm^{-2}, and a superorbital modulation of its X-ray emission with a period of ~14.7 days. The superorbital modulation has been investigated in detail by Islam et al. (2023). These authors showed that the modulation changes in intensity over a time scales of a few years and discussed the results of targeted *NuSTAR* observations (complemented by simultaneous *Swift*/XRT pointings).

IGR J16479–4514 is an eclipsing SFXT with an orbital period of 3.32 days (Jain et al. 2009). The nature of the compact object is unknown because no pulsations have been detected in the system. However, its spectrum is similar to that of accreting HMXB pulsars, suggesting a NS as the putative compact object. The optical companion is likely to be an O7 star, translating into a distance of 4.5 kpc to the binary system (Chaty et al. 2008; Coley et al. 2015). In addition to short low-luminosity X-ray flares lasting a few thousand seconds, orbital phase-locked X-ray flares are present in the light curve, with an occasional bright X-ray flare lasting few hours and reaching an X-ray flux of 10^{-9} erg cm^{-2} s^{-1} (Romano et al. 2008; Sguera et al. 2008; Sidoli et al. 2013; Sguera et al. 2020). These flares suggest the presence of large-scale structures in the stellar wind of the supergiant star (Bozzo et al. 2009; Sguera et al. 2020).

IGR J16493-4348 is an eclipsing high mass X-ray binary with a B0.5 Ia supergiant companion (Nespoli et al. 2010; Pearlman et al. 2019) at ~ 16.1 kpc, and an orbital period of ~ 6.8 d. The X-ray eclipses displayed by the source are known to last about 0.1 d (Cusumano et al. 2010; Corbet et al. 2010a). Given the discovery of X-ray pulsations with a period of 1093 s (Corbet et al. 2010b; Pearlman et al. 2019) and the reported evidence of a resonant cyclotron absorption feature at ~ 30 keV (D'Aì et al. 2011), the compact object hosted in the binary system is believed to be a NS with

a surface magnetic field of 3.7×10^{12} G. A superorbital modulation of the X-ray light curve was discovered by Corbet et al. (2010a) and investigated in depth by Coley et al. (2019).

3 DATA REDUCTION AND ANALYSIS

In order to probe, as a main goal, possible intensity and spectral variability over the superorbital revolution of the NS in 2S 0114+650, we planned our campaign (Target ID 15874, PI: P. Romano) with *Swift*/XRT. The monitoring campaign consisted of 1 ks observations performed 3 times a week starting on 2023-02-10. For this work we considered data collected until 2023-08-24, yielding 74 photon counting (PC) mode observations for a total effective exposure time on the target of 78.8 ks. We adopt for the orbital period P_{orb}=11.5983±0.0006 d (Grundstrom et al. 2007, with the phase zero being the time of periastron passage at MJD 51824.8), and and for the superorbital period P_{sup}=30.76±0.03 d (Corbet & Krimm 2013), with the phase zero being the time of the minimum of the folded light curve, at MJD 53488 (Farrell et al. 2008). Our observations, therefore, cover ~ 17 orbital, and ~ 6 superorbital cycles.

Table A1 reports the log of the *Swift*/XRT observations, including the ObsID, the observation date (MJD of the middle of the observation), the calculated orbital and superorbital phase, the start and end times (UTC), the XRT exposure time, and also relevant spectral parameters (see later in this section).

The XRT data were uniformly processed and analyzed using (FTOOLS[1] v6.29b), and matching calibration (CALDB[2]) files. The spectral analysis was performed with XSPEC (Arnaud 1996), by using the C-statistics Cash (1979) and by adopting an absorbed power-law model with free absorption and photon index. The absorption component was modelled with TBABS) with the default Wilms et al. (2000) abundances (ABUND WILM) and Verner et al. (1996) cross sections (XSECT VERN). Errors on the spectral parameters are reported at the 90 % confidence level (c.l.). The *Swift*/XRT data were analyzed as follows.

First, for each observation we calculated the orbital phase, and from the count rates in the 0.3–4 and 4–10 keV energy bands, we derived the hardness ratio HR = CR(4–10)/CR(0.3–4) (also binned by observation). We extracted the average spectrum and fitted it with an absorbed power law to measure the observed and unabsorbed 0.3–10 keV flux (Cols. 8 and 9 of Table A1).

We then chose eight orbital phase bins that would yield a comparable number of source counts (on average ≈ 2070 cts bin^{-1}) and calculated the HR in those bins. The top panel of Fig. 1 (left) shows the HR in the 8 orbital phase bins, as well as the weighted averages of HRs derived both from individual observations (dotted line) and from the 8 bins (dashed line). We then combined all observations in each of the eight phase bins to create a single spectrum per bin. We note that the number of phase bins was chosen as a compromise between obtaining a significant number of points along the cycle and maintaining a sufficiently high signal-to-noise ratio spectrum to accurately determine both the absorption column density and the power-law slope (see also the discussion in our previous paper, Ferrigno et al. 2022). Finally, we performed an eight-bin phase-resolved spectroscopic analysis in the 0.3–10 keV energy range adopting an absorbed power-law model. The results of our orbital-resolved spectral analysis of 2S 0114+650 are summarized in Table 2 and plotted in Fig. 1 (left).

[1] https://heasarc.gsfc.nasa.gov/ftools/ftools_menu.html.
[2] https://heasarc.gsfc.nasa.gov/docs/heasarc/caldb/caldb_intro.html.

Table 2. Results of the orbital and superorbital phase-resolved spectral analysis for 2S 0114+650.

Phase range	N_H 10^{22} (cm^{-2})	Γ	$F_{0.3-10\,keV}$ 10^{-11} (erg cm^{-2} s^{-1})	Cstat /d.o.f.
Orbital				
0.00–0.15	$2.4^{+0.4}_{-0.3}$	$0.8^{+0.1}_{-0.1}$	$7.6^{+0.4}_{-0.4}$	674.8/694
0.15–0.26	$2.5^{+0.4}_{-0.4}$	$0.7^{+0.1}_{-0.1}$	$14.9^{+0.9}_{-0.8}$	590.9/675
0.26–0.39	$3.8^{+0.5}_{-0.5}$	$0.9^{+0.2}_{-0.2}$	$8.6^{+0.5}_{-0.5}$	634.1/664
0.39–0.55	$6.0^{+0.8}_{-0.7}$	$0.7^{+0.2}_{-0.2}$	$5.2^{+0.3}_{-0.3}$	643.4/664
0.55–0.78	$5.2^{+0.8}_{-0.8}$	$1.0^{+0.2}_{-0.2}$	$3.0^{+0.2}_{-0.2}$	591.1/616
0.78–0.84	$2.7^{+0.4}_{-0.4}$	$0.9^{+0.2}_{-0.1}$	$13.5^{+0.8}_{-0.8}$	604.2/658
0.84–0.92	$2.1^{+0.4}_{-0.3}$	$0.7^{+0.1}_{-0.1}$	$16.0^{+1.0}_{-0.9}$	575.8/638
0.92–0.99	$2.6^{+0.4}_{-0.4}$	$0.9^{+0.2}_{-0.2}$	$8.4^{+0.5}_{-0.5}$	556.0/613
Superorbital				
0.000–0.183	$2.8^{+0.4}_{-0.4}$	$0.9^{+0.2}_{-0.1}$	$3.9^{+0.2}_{-0.2}$	572.7/647
0.183–0.302	$4.1^{+0.5}_{-0.5}$	$1.0^{+0.2}_{-0.2}$	$9.4^{+0.5}_{-0.5}$	649.4/656
0.302–0.450	$3.0^{+0.5}_{-0.4}$	$0.7^{+0.2}_{-0.2}$	$5.9^{+0.4}_{-0.3}$	619.1/667
0.450–0.500	$2.0^{+0.4}_{-0.3}$	$0.6^{+0.1}_{-0.1}$	$25.4^{+1.5}_{-1.4}$	628.4/692
0.500–0.593	$2.9^{+0.5}_{-0.4}$	$0.6^{+0.2}_{-0.1}$	$10.4^{+0.6}_{-0.6}$	674.8/673
0.593–0.820	$2.5^{+0.4}_{-0.4}$	$0.9^{+0.1}_{-0.1}$	$6.5^{+0.4}_{-0.4}$	701.4/673
0.820–0.880	$3.9^{+0.6}_{-0.6}$	$0.8^{+0.2}_{-0.2}$	$7.1^{+0.5}_{-0.5}$	474.0/610
0.880–1.000	$4.0^{+0.6}_{-0.6}$	$0.7^{+0.2}_{-0.2}$	$6.1^{+0.4}_{-0.3}$	613.1/645

We repeated the same procedure for the creation of superorbital phase bins and the corresponding spectroscopic analysis. The results are reported in Table 2 and Fig. 1 (right). Finally, in Appendix B we also address the effect of data binning on our result.

We note that the use of a simple model comprising an absorption component and a power law is justified for the source based on previous work (see Sect. 2.1), due to the limited energy band coverage and exposure of the stacked XRT spectra. The addition of a cut-off energy, as measured by *RXTE* and *Suzaku*, at energies 10–30 keV (Farrell et al. 2008; Abdallah et al. 2023) was tested and found not to significantly affect the results obtained here. More complicated models including Comptonizing components and reported in a few studies exploiting either the broad-band coverage of the instruments on-board *Suzaku* or the deep exposures of the *XMM-Newton* data (Pradhan et al. 2015; Sanjurjo-Ferrrín et al. 2017) were also not usable in the present case, as most parameters would simply be unconstrained. As our scope is to unveil the relative variability between observations carried out with the same instrument at different orbital and super-orbital phases, the absorbed power-law model allows us to unveil if the variability is mostly occurring in the soft X-ray part of the spectrum (and thus most likely associated with the absorption column density) or driven by changes in the harder part of the XRT energy band (thus more likely associated by a change in the overall spectral slope). As a further remark, we note that the procedure we adopted here also ensures that the known (modest) spectral energy variability due to the energy-dependent pulsations from the source is averaged out in the stacked XRT spectra (see Pradhan et al. 2015, and references therein, and Appendix B). This is because for each orbital and superorbital bin we are merging together many different relatively short XRT pointings (typically 1–2 ks at most) over sev-

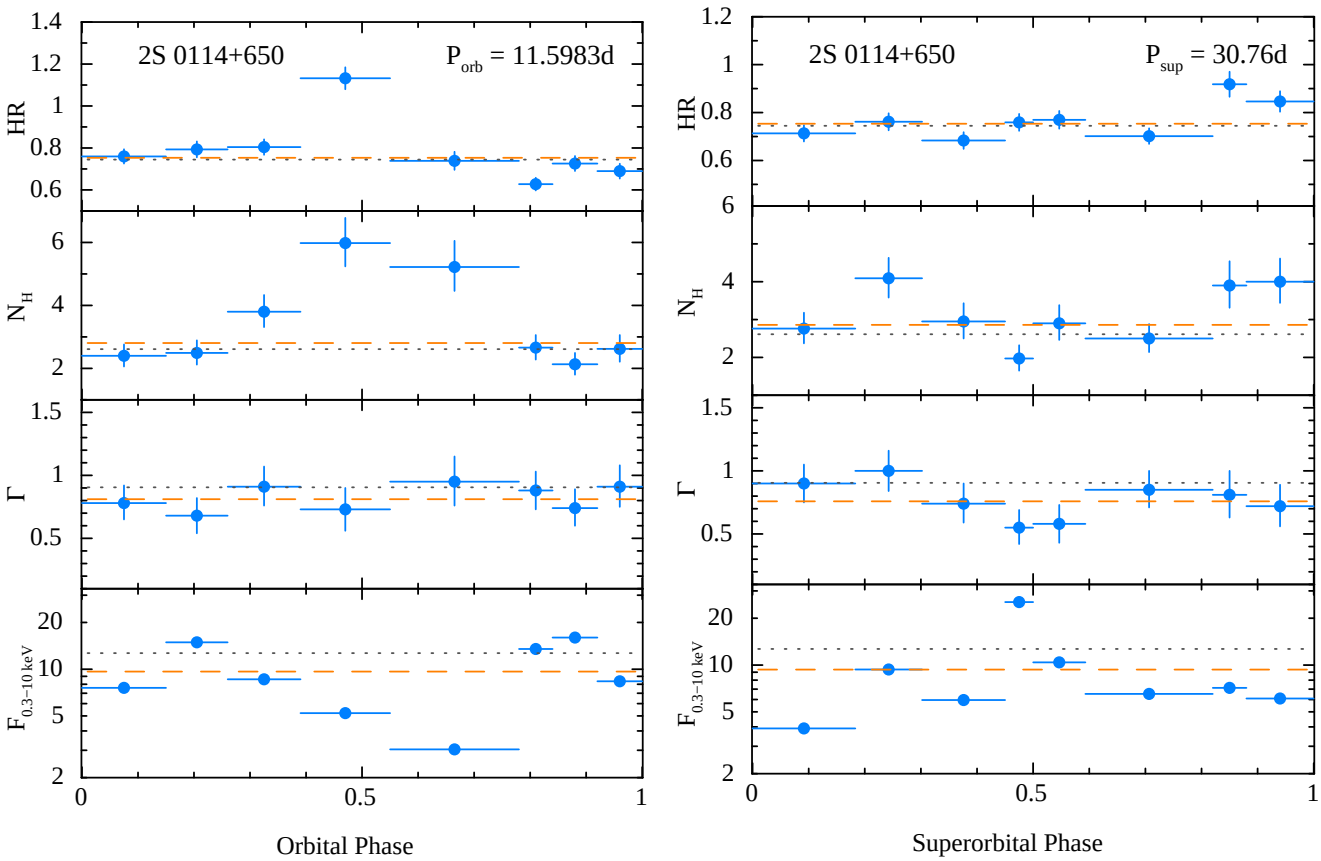

Figure 1. *Left*: *Swift*/XRT hardness ratio of 2S 0114+650, and best-fit parameters as a function of orbital phase (P_{orb}=11.5983 d, T_0= MJD 51824.8). The absorption column density N_H is in units of 10^{22} cm^{-2}, the power-law photon index is Γ, and the observed 0.3–10 keV flux is in units of 10^{-11} erg cm^{-2} s^{-1}). *Right*: same as left side but for the superorbital phase (P_{sup}=30.76 d, T_0= MJD 53488, Corbet & Krimm 2013). In each panel we also report the mean value of each variable plotted when calculated from the individual observations (dotted line) and from the values obtained in the eight phase bins (orange dashed line). The two lines are compatible in all cases within the associated uncertainties.

eral different orbital and superorbital revolutions (see Appendix B for futhr details).

For completeness, we applied the methodology of folding along the superorbital phase to three more sources, listed in Table 1 along with their relevant properties, IGR J16418−4532, IGR J16479−4514, and IGR J16493−4348. For these sources, the data available in the *Swift* archive were not optimized to investigate superorbital spectral variations but rather obtained either as monitoring campaigns for the orbital variability or as SFXT discovery/outburst follow-ups (see Romano et al. 2023). Spectral variations as a function of the orbital phase of these three sources were already investigated in previous work (see Romano et al. 2012a; Sidoli et al. 2013; Varun & Raman 2023; Pearlman et al. 2019, and references therein). In order to optimise the *Swift* archival data for superorbital variability studies, we selected only observations with homogeneous exposure times, so as not to introduce biases in favour of a specific superorbital phase, and with an off-axis angle < 15′ to limit the known XRT vignetting effects. We then applied the same procedures as those adopted for 2S 0114+650, as follows.

The data we considered for IGR J16418−4532 are reported in Table A2. The majority have mostly been collected either as monitoring campaigns (e.g. Romano et al. 2012a) or as outburst follow-ups (Romano et al. 2023, and references therein, and in Table A2). Consequently, their exposures vary considerably, from ∼2–5 ks obtained during the orbital monitoring in 2011 (Romano et al. 2012a) that uniformly cover three orbital periods (1.1 superorbital periods), or ∼2 ks triggered observations and their follow-up campaigns (typically 1 ks per observation), to very short serendipitous observations. By combining all the data (57 observations for a total exposure of 93 ks) we obtained eight phase-selected spectra with an average of ≈ 900 counts each, the only exception being bin number five, where only one observation (00032037022) was available which did not even yield a detection.

For IGR J16479−4514, we considered the data published in Romano et al. (2009, Table 5) and in Romano et al. (2011, Table 1), that were collected to define the long term properties of a sample of SFXTs (Sidoli et al. 2008; Romano et al. 2008; Sidoli et al. 2009; Romano et al. 2009, 2011). The campaign consisted of 144 observations, each 1 ks long, obtained twice a week, along a baseline of two yearas well as outburst observations and their follow-ups, for a total of ∼160 ks. The observations cover ∼ 54 superorbital cycles[3] and yield eight phase-selected spectra with ≈ 1650 counts each.

Finally, for IGR J16493−4348, we considered the monitoring data we obtained in 2014 (see Table A4) to study the long term behaviour of this source and create the cumulative luminosity distribution, with

[3] We discarded observation 00030296005, since it is a single observation dated three months before the remainder of the campaign.

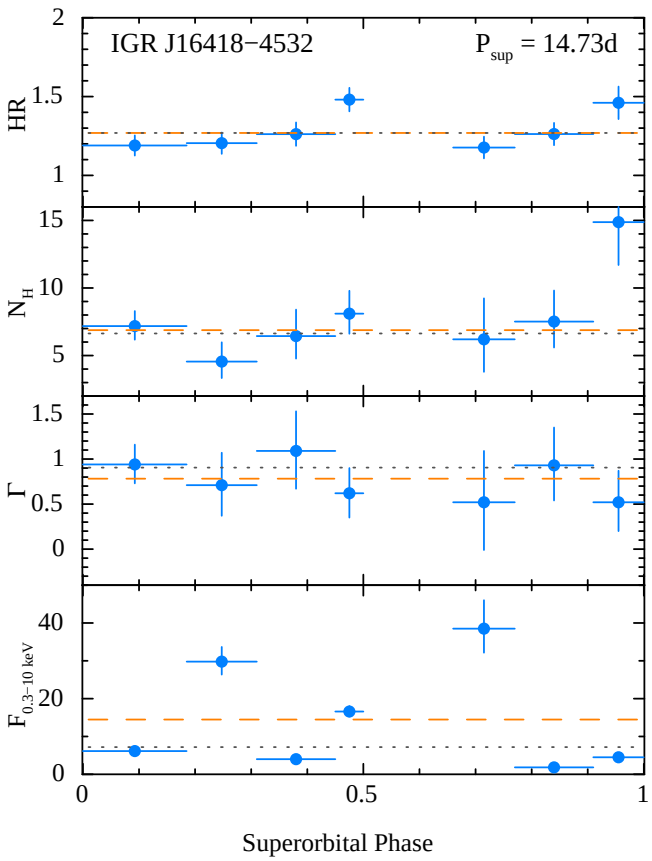

Figure 2. Same as Fig. 1 (right) but for the case of IGR J16418−4532 (P_{sup}=14.730 d, T_0= 55994.6 MJD, Corbet & Krimm 2013).

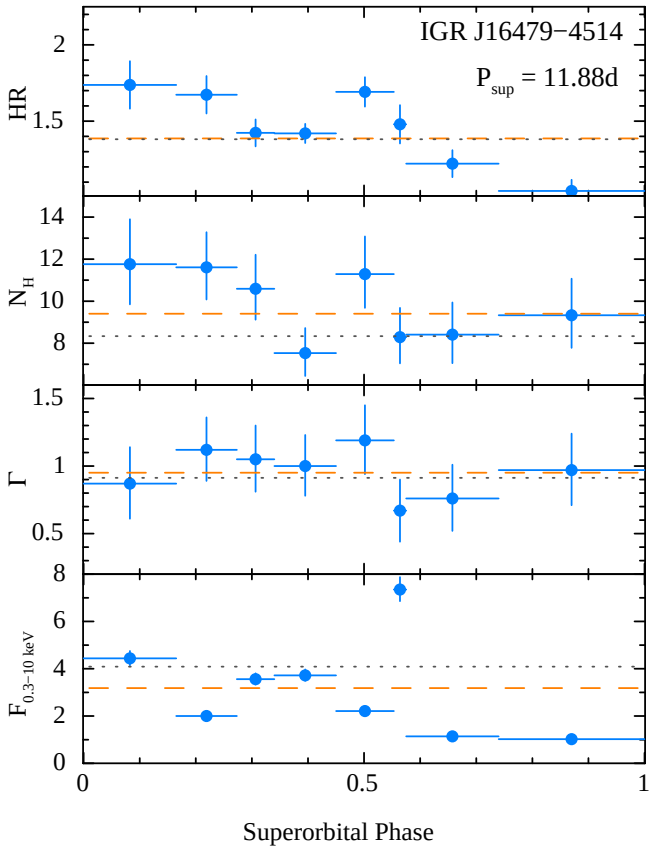

Figure 3. Same as Fig. 1 (right) but for the case of IGR J16479−4514 (P_{sup}=11.880 d, T_0= MJD 55996, Corbet & Krimm 2013).

a cadence of 1 ks twice a week for a total of ~53 ks and 57 observations, as reported in Romano (2015) and Kretschmar et al. (2019). These observations, covering ~ 11 superorbital cycles, yield eight phase-selected spectra with ≈ 700 counts each.

Figures 2, 3, and 4 show the HR and best-fit parameters as a function of superorbital phase for IGR J16418−4532, IGR J16479−4514, and IGR J16493−4348, respectively, while the values of the best fit parameters are reported in Table 3.

4 RESULTS AND DISCUSSION

4.1 Orbital variability

The suitability of XRT monitoring campaigns to perform orbital variability studies was already widely demonstrated by our group in a recent paper for a number of wind-fed binaries (Ferrigno et al. 2022). Here we discuss the orbital variability only for the source 2S 0114+650, as for the remaining sources considered in the present paper the corresponding results were already reported previously by our group and also extensively analyzed in the literature (see Romano et al. 2009, 2011, 2012a, and references therein).

The left side of Fig. 1 shows the variability of the spectral parameters measured in the case of 2S 0114+650 as a function of the system orbital phase. As in the case of previous objects, XRT was able to unveil also for this source an interesting variability pattern for the flux, the absorption column density, and the power-law photon index. The phase 0 is set at the periastron passage in such a way that our figure and the equivalent one realized with *Swift*/BAT data (15–50 keV) in Corbet & Krimm (2013, see their Fig. 2) are directly comparable. Both lightcurves display a minimum in flux at phase 0.7 that was already visible in the folded *RXTE*/PCA data[4] (2–12 keV range) reported by Farrell et al. (see their Fig. 13; 2008) and extensively investigated by Pradhan et al. (2015) to verify the hypothesis of an X-ray eclipse. The latter authors concluded that the properties of the flux minimum are not compatible with being a total obscuration of the NS by its companion. This conclusion was mainly driven by the fact that *Suzaku* data collected during the flux minimum could only reveal a modest increase of the local column density (a factor of ~ 3) and equivalent width of the fluorescence iron line (if any at all), as well as a complete lack of evidence for a significant flattening of the spectral slope. This is at odds with what is commonly observed in eclipsing wind-fed X-ray binaries where both the absorption column density and equivalent width of the fluorescence iron emission line can increase by a factor of ~10–100 (compared to the out-of-eclipse emission), and the power-law slope gets dramatically softer due to the fact that only the scattered X-ray emission is observed during the eclipse (rather than the direct X-ray emission from the accreting source; see, e.g. Falanga et al. 2015, and references therein). These authors thus suggested that the flux

[4] Note that the source light curve folded on the system orbital period reported in Farrell et al. (2008) uses the time of the flux minimum to define phase 0 and thus there is a shift of ~0.3 in phase compared to our and Corbet & Krimm (2013) light curves.

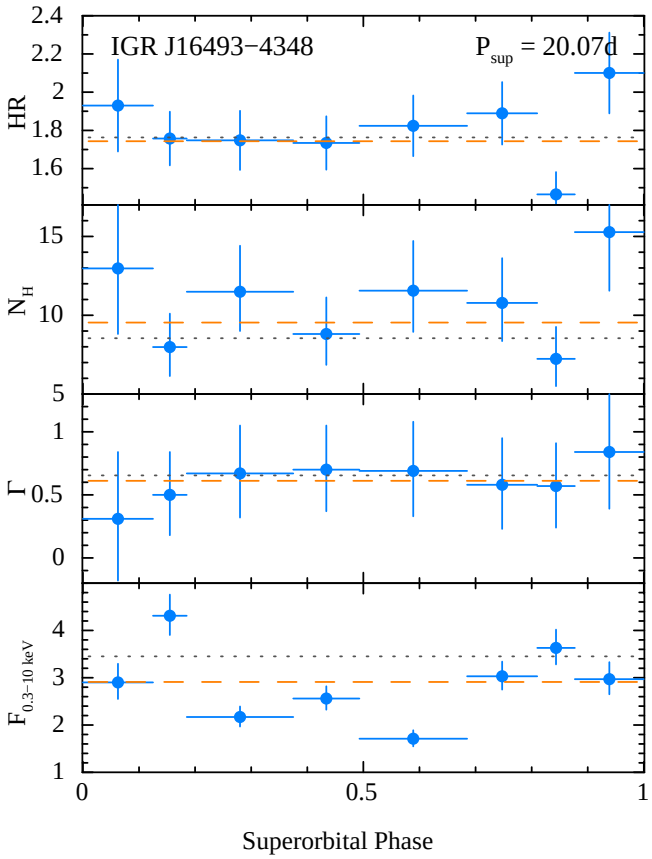

Figure 4. Same as Fig. 1 (right) but for the case of IGR J16493−4348 (P_{sup}=20.07 d, T_0= MJD 54265.1, Corbet & Krimm 2013; Coley et al. 2015).

minimum is most likely due to the modulation of the mass accretion rate along the relatively highly eccentric orbit (see Sect. 2.1). The sensitivity achieved thanks to our XRT monitoring campaign allows us to confirm this suggestion, since during the flux minimum we recorded a noticeable but still modest increase of N_H compared to the remaining orbital phases (a factor of ~3 as reported also by Pradhan et al. 2015). We can consider that the XRT measurement is truly representative of the characteristic absorption column density in the X-ray dip because this value is obtained as an average of many different orbital cycles.

The folded XRT lightcurve also presents two peaks in flux preceding and following the periastron passage. Although this has not been widely discussed in the literature, it is worth remarking that the peak in flux following the periastron is expected in case of eccentric or short-orbital period wind-fed SgXB due to the effect of both the stellar wind photoionization by the high-energy emission of the compact object and the relative velocity between the orbiting NS and the stellar wind. As a consequence of these effects, a second peak in flux is also expected slightly before the NS approaches the periastron again (with the exact position in phase depending also on the poorly known physical conditions of the stellar wind, as the density, velocity, and ionization state; see Bozzo et al. 2021, and references therein). A similar double peaked lightcurve is observed in the case of the SFXT endowed with the shortest orbital period of this class of objects, IGR J16479-4514 (Sidoli et al. 2013, Fig. 1).

Note that the double peaked structure of the folded XRT lightcurve is not immediately evident from the equivalent folded lightcurves in the higher energy domains, e.g. those obtained from *Swift*/BAT. This is not unexpected as the X-ray emission of wind-fed SgXBs above ≳10 keV is dominated by the cut-off power-law spectral component. This component usually shows a much less pronounced variability along the orbital phase (see also the discussion in Farrell et al. 2008) and it is only marginally affected by changes in the absorption column density local to the source. The folded BAT lightcurves along the orbital phases of SgXBs thus display in most of the cases a modest (if any at all) variability, apart from the evident cases of X-ray eclipses (see Falanga et al. 2015; Coley et al. 2015, for recent reviews). Before the provision of our XRT results here, a very different profile of the X-ray emission from 2S 0114+650 in the soft versus hard X-ray domain could be well appreciated by looking at Fig. 2 of Pradhan et al. (2015). Although the *Suzaku*/XIS data covering the soft energy domain (≲10 keV) only spanned a limited portion of the orbital phase around the X-ray minimum, the much more prominent variability of these data compared to the super-imposed ones from *Swift*/BAT is particularly striking.

Table 3. Results of the superorbital phase-resolved spectral analysis for the three sources IGR J16418−4532, IGR J16479−4514, and IGR J16493−4348.

Superorbital phase	N_H 10^{22} (cm^{-2})	Γ	$F_{0.3-10keV}$ 10^{-11} (erg cm^{-2} s^{-1})	Cstat /d.o.f.
J16418				
0.000–0.185	$7.2^{+1.1}_{-1.0}$	$0.9^{+0.2}_{-0.2}$	$6.1^{+0.4}_{-0.4}$	556.0/608
0.185–0.310	$4.5^{+1.4}_{-1.2}$	$0.7^{+0.4}_{-0.3}$	$29.8^{+3.9}_{-3.4}$	269.3/327
0.310–0.450	$6.4^{+2.0}_{-1.7}$	$1.1^{+0.4}_{-0.4}$	$4.0^{+0.6}_{-0.5}$	263.3/294
0.450–0.500	$8.1^{+1.7}_{-1.5}$	$0.6^{+0.3}_{-0.3}$	$16.6^{+1.4}_{-1.3}$	435.5/514
0.500–0.660	–	–	–	–
0.660–0.770	$6.2^{+3.0}_{-2.4}$	$0.5^{+0.6}_{-0.5}$	$38.5^{+7.5}_{-6.4}$	163.5/181
0.770–0.910	$7.5^{+2.3}_{-1.9}$	$0.9^{+0.4}_{-0.4}$	$1.8^{+0.2}_{-0.2}$	304.5/374
0.910–1.000	$14.9^{+3.8}_{-3.2}$	$0.5^{+0.3}_{-0.3}$	$4.5^{+0.3}_{-0.3}$	551.0/596
J16479				
0.000–0.165	$11.8^{+2.1}_{-1.9}$	$0.9^{+0.3}_{-0.3}$	$4.4^{+0.3}_{-0.3}$	542.5/582
0.165–0.273	$11.6^{+1.7}_{-1.5}$	$1.1^{+0.2}_{-0.2}$	$2.0^{+0.1}_{-0.1}$	576.6/624
0.273–0.340	$10.6^{+1.6}_{-1.5}$	$1.1^{+0.2}_{-0.2}$	$3.6^{+0.2}_{-0.2}$	500.6/591
0.340–0.450	$7.5^{+1.2}_{-1.1}$	$1.0^{+0.2}_{-0.2}$	$3.7^{+0.3}_{-0.2}$	596.2/593
0.450–0.553	$11.3^{+1.8}_{-1.6}$	$1.2^{+0.3}_{-0.3}$	$2.2^{+0.2}_{-0.1}$	495.2/580
0.553–0.575	$8.3^{+1.4}_{-1.3}$	$0.7^{+0.2}_{-0.2}$	$7.4^{+0.5}_{-0.5}$	533.4/585
0.575–0.740	$8.4^{+1.5}_{-1.4}$	$0.8^{+0.3}_{-0.2}$	$1.1^{+0.1}_{-0.1}$	498.0/574
0.740–1.000	$9.3^{+1.7}_{-1.6}$	$1.0^{+0.3}_{-0.3}$	$1.0^{+0.1}_{-0.1}$	494.0/572
J16493				
0.000–0.125	$13.0^{+5.1}_{-4.2}$	$0.3^{+0.5}_{-0.5}$	$2.9^{+0.4}_{-0.3}$	275.8/332
0.125–0.185	$8.0^{+2.1}_{-1.8}$	$0.5^{+0.3}_{-0.3}$	$4.3^{+0.4}_{-0.4}$	338.7/416
0.185–0.375	$11.5^{+2.9}_{-2.5}$	$0.7^{+0.4}_{-0.4}$	$2.2^{+0.2}_{-0.2}$	377.8/443
0.375–0.493	$8.8^{+2.3}_{-2.0}$	$0.7^{+0.4}_{-0.3}$	$2.6^{+0.3}_{-0.2}$	357.0/437
0.493–0.685	$11.6^{+3.1}_{-2.6}$	$0.7^{+0.4}_{-0.4}$	$1.7^{+0.2}_{-0.2}$	324.3/435
0.685–0.810	$10.8^{+2.8}_{-2.4}$	$0.6^{+0.4}_{-0.3}$	$3.0^{+0.3}_{-0.3}$	378.7/420
0.810–0.877	$7.2^{+2.0}_{-1.7}$	$0.6^{+0.3}_{-0.3}$	$3.6^{+0.4}_{-0.3}$	344.3/425
0.877–1.000	$15.3^{+4.3}_{-3.7}$	$0.8^{+0.5}_{-0.5}$	$3.0^{+0.4}_{-0.3}$	277.5/361

4.2 Superorbital variability

Of more interest for the focus of this paper are the variations of the source spectral parameters as a function of the superorbital phase, as shown in the right side of Fig. 1. In the past, only Farrell et al. (2008) attempted a superorbital-phase-resolved spectral analysis of the X-ray emission from 2S 0114+650, but the outcomes of their analysis were partly hampered by the limited coverage of the *RXTE*/PCA data used, which sampled only two superorbital cycles. The PCA folded light curve showed a peak of the emission at phase 0.5, and only a marginally significant increase in the photon index was reported around phase 1.0. The data also suggested a possible increase of the absorption column density at the same phase, but the uncertainty associated with the measurement was far too large to draw a firm conclusion. The higher sensitivity and longer coverage of our XRT monitoring campaign (spanning six superorbital cycles) allows us to improve the measurements and investigate in more detail the properties of the source X-ray emission at different superorbital phases. The profile of the XRT folded light curve shows a sharp peak in the source flux at phase 0.5 and an intriguing pattern of variability of the $N_{\rm H}$, confirming a remarkable increase toward phase 0.8–1.0 (note that our figure and Fig. 16 of Farrell et al. (2008) are directly compatible as the reference time for phase 0 is the same in both cases). We could not detect any changes in the power-law photon index, which remains virtually constant at a value of 0.8 at most superorbital phases and show a modest decrease down to ~0.6 around the superorbital phase 0.5. We tested that a fit to the eight superorbital phase bin spectra with a common photon index (introducing inter-calibration constants and with all other parameters free) yields a photon index of $0.795^{+0.056}_{-0.055}$, which is consistent with all individual fits apart from the two spectra extracted around phase 0.5. However, in these two cases, the deviation is only marginally ($\lesssim 3\ \sigma$ c.l.) significant.

Farrell et al. (2008) suggested that the superorbital periodicity in 2S 0114+650 could be due to a periodic variation of the mass accretion rate, although these authors could not identify any specific mechanism(s) driving the variation. As discussed in Sect. 1, there is a general convergence in believing that the CIR model provides the most solid ground to explain the superorbital variability of wind-fed X-ray binaries as 2S 0114+650. In this model, increases in the flux are associated with the accretion onto the NS of the denser (by a factor of 2–3; see Lobel & Blomme 2008, and reference stherein) and (possibly) slower material of the CIR compared to the surrounding stellar wind. This interaction should also lead to increases in the local absorption column density, because the CIR is expected to intercept at some point the line of sight between the compact object and the observer. Our XRT measurements unveiled increases in the flux and absorption column density that are compatible with the factor 2–3 expected in the CIR model, although some geometrical effect shall be assumed in order to interpret the difference in phase between the rise in the flux and that in the $N_{\rm H}$. Compatibly with the CIR model, no dramatic variation is observed in the power-law photon index, as accretion is driven at any phase by the stellar wind and no spectral state changes are expected as those observed in disk-accreting systems (Bozzo et al. 2016). In view of the pioneering measurements we presented with XRT, it is difficult to obtain insights into the possibility suggested by Hu et al. (2017) that the source is not a pure wind-fed system but a temporary accretion disk is forming around the NS when the super-orbital variability is more pronounced. The physics of temporary accretion disk formation around NS in wind-fed binaries is not yet known, and neither are the expected spectral energy variations as a function of the accretion disk properties (see, e.g., the discussion in Romano et al. 2015). However, should a temporary accretion disk be driving the super-orbital modulation in 2S 0114+650, one would likely expect to see spectral state changes (i.e., changes in the power-law photon index) at different superorbital phases as those recorded from, e.g. Her X-1 and SMC X-1 (see, e.g., Brumback et al. 2021, 2023, and references therein). At present, our XRT data do not show clear evidence to support this but deeper and more extended observations of the source are clearly needed to consolidate the reported findings (to be carried out by exploiting, e.g., the combination of flexibility, soft X-ray coverage, and large effective area of NICER, Gendreau et al. 2012).

Concerning the remaining three sources considered in this paper, we note that in the case of IGR J16418−4532, XRT revealed some intriguing variability pattern for the source flux as a function of the superorbital phase (see Fig. 2). However, the coverage in phase is not complete and the S/N in the different available bins is far too low to claim the detection of any meaningful variation in either the power-law photon index or the absorption column density. We tested that merging more phase bins together to increase the S/N would not allow us to have a reasonable number of points to search for spectral variations at different superorbital phases. In the case of IGR J16479−4514, the intriguing flux pattern is also accompanied by a similar HR variability trend. There is some indication in the data for possible variations especially of the absorption column density, but more data are needed in the different phase bins in order to decrease the uncertainties on the spectral parameters and draw a more firm conclusion. Among all analyzed sources, IGR J16493−4348 is the least interesting from a superorbital analysis point of view. XRT could only reveal modest changes in the flux and did not provide indications for possible variations in either the absorption column density or the power-law photon index. It should be noted, however, that the source is relatively faint for XRT and the error bars associated with both $N_{\rm H}$ and Γ are definitively larger than in other cases (thus hampering any attempt to unveil only modest variations of these parameters). A substantially larger number of observations would be needed in this case to lower the error bars and dig into the presence of possibly modest (but recurrent) variations of the source spectral parameters as a function of the superorbital phase.

DATA AVAILABILITY

The data underlying this article are publicly available from the *Swift* archive and processed with publicly available software.

ACKNOWLEDGEMENTS

We acknowledge unwavering support from Amos. We also thank the anonymous referee for comments that helped improve the paper. We acknowledge financial contribution from contracts ASI-INAF I/037/12/0 and ASI-INAF n. 2017-14-H.0. NI acknowledges support from NASA grants 80NSSC21K0022 and 80NSSC21K1994. This work was supported in part by NASA under award number 80GSFC21M0002. The *Swift* data of our monitoring campaigns on 2S 0114+650, on IGR J16493−4348 and (partially) IGR J16418−4532 were obtained through contract ASI-INAF I/004/11/0 to ASI-INAF I/004/11/5. This work made use of data supplied by the UK Swift Science Data Centre at the University of Leicester (see Evans et al. 2007, 2009). Happy 18th, *Swift*.

REFERENCES

Abdallah M. H., Samir R. M., Leahy D. A., Shaker A. A., 2023, MNRAS, 522, 3271

Ambrosi E., D'Aì A., Del Santo M., Segreto A., Ferrigno C., Amato R., Cusumano G., 2022, MNRAS, 512, 3422

Arnaud K. A., 1996, in Jacoby G. H., Barnes J., eds, Astronomical Society of the Pacific Conference Series Vol. 101, Astronomical Data Analysis Software and Systems V. p. 17

Bozzo E., Giunta A., Stella L., Falanga M., Israel G., Campana S., 2009, A&A, 502, 21

Bozzo E., Oskinova L., Feldmeier A., Falanga M., 2016, A&A, 589, A102

Bozzo E., Oskinova L., Lobel A., Hamann W. R., 2017, A&A, 606, L10

Bozzo E., Ducci L., Falanga M., 2021, MNRAS, 501, 2403

Brumback M. C., Hickox R. C., Fürst F. S., Pottschmidt K., Tomsick J. A., Wilms J., 2020, ApJ, 888, 125

Brumback M. C., Hickox R. C., Fürst F. S., Pottschmidt K., Tomsick J. A., Wilms J., Staubert R., Vrtilek S., 2021, ApJ, 909, 186

Brumback M. C., Vasilopoulos G., Coley J. B., Dage K., Miller J. M., 2023, ApJ, 953, 89

Burrows D. N., et al., 2005, Space Sci. Rev., 120, 165

Cash W., 1979, ApJ, 228, 939

Chaty S., Rahoui F., Foellmi C., Tomsick J. A., Rodriguez J., Walter R., 2008, A&A, 484, 783

Coleiro A., Chaty S., Zurita Heras J. A., Rahoui F., Tomsick J. A., 2013, A&A, 560, A108

Coley J. B., Corbet R. H. D., Krimm H. A., 2015, ApJ, 808, 140

Coley J. B., Corbet R. H. D., Fürst F., Huxtable G., Krimm H. A., Pearlman A. B., Pottschmidt K., 2019, ApJ, 879, 34

Corbet R. H. D., Krimm H. A., 2013, ApJ, 778, 45

Corbet R. H. D., Barthelmy S. D., Baumgartner W. H., Krimm H. A., Markwardt C. B., Skinner G. K., Tueller J., 2010a, The Astronomer's Telegram, 2599, 1

Corbet R. H. D., Pearlman A. B., Pottschmidt K., 2010b, The Astronomer's Telegram, 2766, 1

Corbet R. H. D., Coley J. B., Krimm H. A., 2017, ApJ, 846, 161

Corbet R. H. D., Coley J. B., Krimm H. A., Pottschmidt K., Roche P., 2021, ApJ, 906, 13

Cusumano G., La Parola V., Romano P., Segreto A., Vercellone S., Chincarini G., 2010, MNRAS, 406, L16

D'Aì A., Cusumano G., La Parola V., Segreto A., di Salvo T., Iaria R., Robba N. R., 2011, A&A, 532, A73

Doroshenko V., Santangelo A., Nakahira S., Mihara T., Sugizaki M., Matsuoka M., Nakajima M., Makishima K., 2013, A&A, 554, A37

Dower R., Kelley R., Margon B., Bradt H., 1977, IAU Circ., 3144, 2

Ducci L., Sidoli L., Paizis A., 2010, MNRAS, 408, 1540

Evans P. A., et al., 2007, A&A, 469, 379

Evans P. A., et al., 2009, MNRAS, 397, 1177

Falanga M., Bozzo E., Lutovinov A., Bonnet-Bidaud J. M., Fetisova Y., Puls J., 2015, A&A, 577, A130

Farrell S. A., Sood R. K., O'Neill P. M., 2006, MNRAS, 367, 1457

Farrell S. A., Sood R. K., O'Neill P. M., Dieters S., 2008, MNRAS, 389, 608

Ferrigno C., Bozzo E., Romano P., 2022, A&A, 664, A99

Gehrels N., et al., 2004, ApJ, 611, 1005

Gendreau K. C., Arzoumanian Z., Okajima T., 2012, in Takahashi T., Murray S. S., den Herder J.-W. A., eds, Vol. 8443, Space Telescopes and Instrumentation 2012: Ultraviolet to Gamma Ray. SPIE, p. 844313, doi:10.1117/12.926396, https://doi.org/10.1117/12.926396

Grundstrom E. D., et al., 2007, ApJ, 656, 431

Hall T. A., Finley J. P., Corbet R. H. D., Thomas R. C., 2000, ApJ, 536, 450

Hu C.-P., Chou Y., Ng C. Y., Lin L. C.-C., Yen D. C.-C., 2017, ApJ, 844, 16

Islam N., Paul B., 2014, MNRAS, 441, 2539

Islam N., Corbet R. H. D., Coley J. B., Pottschmidt K., Fuerst F., 2023, ApJ, 948, 45

Jain C., Paul B., Dutta A., 2009, MNRAS, 397, L11

Koenigsberger G., Moreno E., Cervantes F., 2003, in van der Hucht K., Herrero A., Esteban C., eds, Vol. 212, A Massive Star Odyssey: From Main Sequence to Supernova. p. 101

Koenigsberger G., Georgiev L., Moreno E., Richer M. G., Toledano O., Canalizo G., Arrieta A., 2006, A&A, 458, 513

Kretschmar P., et al., 2019, New Astron. Rev., 86, 101546

Krimm H. A., et al., 2013, The Astronomer's Telegram, 5398, 1

Levine A. M., Bradt H. V., Chakrabarty D., Corbet R. H. D., Harris R. J., 2011, ApJS, 196, 6

Lobel A., Blomme R., 2008, ApJ, 678, 408

Martínez-Núñez S., et al., 2017, Space Sci. Rev., 212, 59

Matsuoka M., Kawasaki K., Ueno S., Tomida H., Kohama M., Suzuki M., Adachi Y., Ishikawa M. X. e. a., 2009, PASJ, 61, 999

Moreno E., Koenigsberger G., Toledano O., 2005, A&A, 437, 641

Moreno E., Koenigsberger G., Harrington D. M., 2011, A&A, 528, A48

Nespoli E., Fabregat J., Mennickent R. E., 2010, A&A, 516, A106

Pearlman A. B., Coley J. B., Corbet R. H. D., Pottschmidt K., 2019, ApJ, 873, 86

Pradhan P., Paul B., Paul B. C., Bozzo E., Belloni T. M., 2015, MNRAS, 454, 4467

Pradhan P., Maitra C., Paul B., 2020, ApJ, 895, 10

Reig P., Chakrabarty D., Coe M. J., Fabregat J., Negueruela I., Prince T. A., Roche P., Steele I. A., 1996, A&A, 311, 879

Rodes-Roca J. J., Mihara T., Nakahira S., Torrejón J. M., Giménez-García Á., Bernabéu G., 2015, A&A, 580, A140

Romano P., 2015, Journal of High Energy Astrophysics, 7, 126

Romano P., et al., 2008, ApJ, 680, L137

Romano P., et al., 2009, MNRAS, 399, 2021

Romano P., et al., 2011, MNRAS, 410, 1825

Romano P., et al., 2012a, MNRAS, 419, 2695

Romano P., et al., 2012b, The Astronomer's Telegram, 4148, 1

Romano P., et al., 2013, Mem. Soc. Astron. Italiana, 84, 602

Romano P., et al., 2014, A&A, 562, A2

Romano P., et al., 2015, A&A, 576, L4

Romano P., et al., 2023, A&A, 670, A127

Sanjurjo-Ferrrín G., Torrejón J. M., Postnov K., Oskinova L., Rodes-Roca J. J., Bernabeu G., 2017, A&A, 606, A145

Sbarufatti B., Romano P., Barthelmy S. D., Krimm H. A., Evans P. A., Kennea J. A., Page K. L., Siegel M. H., 2021, The Astronomer's Telegram, 14924, 1

Sguera V., et al., 2006, ApJ, 646, 452

Sguera V., et al., 2008, A&A, 487, 619

Sguera V., Tiengo A., Sidoli L., Bird A. J., 2020, ApJ, 900, 22

Sidoli L., et al., 2008, ApJ, 687, 1230

Sidoli L., et al., 2009, ApJ, 690, 120

Sidoli L., Mereghetti S., Sguera V., Pizzolato F., 2012, MNRAS, 420, 554

Sidoli L., et al., 2013, MNRAS, 429, 2763

Sood R., Farrell S., O'Neill P., Dieters S., 2007, Advances in Space Research, 40, 1528

Tomsick J. A., Lingenfelter R., Corbel S., Goldwurm A., Kaaret P., 2004, The Astronomer's Telegram, 224, 1

Varun Raman G., 2023, MNRAS, 523, 5024

Verner D. A., Ferland G. J., Korista K. T., Yakovlev D. G., 1996, ApJ, 465, 487

Walter R., Lutovinov A. A., Bozzo E., Tsygankov S. S., 2015, A&ARv, 23, 2

Wilms J., Allen A., McCray R., 2000, ApJ, 542, 914

APPENDIX A: LOGS OF OBSERVATIONS

In this Section we include several tables to complement the results described in the main paper. Table A1 reports all details of the new observational campaign focused on 2S 0114+650 (and never reported elsewhere), while Tables A2, A3, and A4 those of the campaigns on IGR J16418−4532, IGR J16479−4514, and IGR J16493−4348.

Table A1. Observation log for 2S 0114+650: ObsID, date (MJD of the middle of the observation), orbital phase, superorbital phase, start and end times (UTC), XRT exposure time, and 0.3–10 keV observed and unabsorbed flux.

ObsID	MJD	Orbital[a] Phase	Super-o.[b] Phase	Start time (UT) (yyyy-mm-dd hh:mm:ss)	End time (UT) (yyyy-mm-dd hh:mm:ss)	Exposure (s)	Flux[c] (erg cm^{-2} s^{-1})	Flux[d] (erg cm^{-2} s^{-1})
00015874001	59985.97953	0.65	0.25	2023-02-10 23:23:09	2023-02-10 23:37:52	883	$2.5^{+0.8}_{-0.6}$	$13.7^{+11.5}_{-8.6}$
00015874002	59987.63298	0.80	0.30	2023-02-12 15:05:05	2023-02-12 15:17:52	767	$21.3^{+3.3}_{-2.8}$	$28.4^{+4.4}_{-3.1}$
00015874003	59989.36260	0.94	0.36	2023-02-14 08:34:24	2023-02-14 08:49:52	928	$1.2^{+0.4}_{-0.3}$	$1.7^{+0.8}_{-0.4}$
00015874004	59992.53420	0.22	0.46	2023-02-17 12:40:37	2023-02-17 12:57:52	1036	$55.8^{+5.8}_{-5.2}$	$63.2^{+5.1}_{-4.7}$
00015874005	59994.18332	0.36	0.51	2023-02-19 04:17:05	2023-02-19 04:30:52	827	$36.1^{+4.4}_{-3.9}$	$43.4^{+4.0}_{-3.7}$
00015874006	59996.17138	0.53	0.58	2023-02-21 03:59:42	2023-02-21 04:13:52	850	$21.3^{+4.0}_{-3.4}$	$52.8^{+19.8}_{-16.8}$
00015874007	59999.09258	0.78	0.67	2023-02-24 02:05:43	2023-02-24 02:20:53	910	$16.3^{+3.2}_{-2.6}$	$22.7^{+6.3}_{-3.3}$
00015874008	60001.14424	0.96	0.74	2023-02-26 03:20:31	2023-02-26 03:34:53	863	$2.4^{+0.6}_{-0.5}$	$3.7^{+2.4}_{-0.8}$
00015874009	60003.59002	0.17	0.82	2023-02-28 14:05:20	2023-02-28 14:13:54	514	$7.1^{+1.4}_{-1.2}$	$9.0^{+1.6}_{-1.2}$
00015874010	60006.39117	0.41	0.91	2023-03-03 00:34:40	2023-03-03 18:11:53	1860	$8.7^{+1.1}_{-1.0}$	$12.9^{+2.4}_{-1.4}$
00015874011	60009.07858	0.64	1.00	2023-03-05 06:44:26	2023-03-06 21:01:53	3229	–	–
00015874012	60010.53555	0.77	0.05	2023-03-07 01:42:29	2023-03-07 23:59:53	3543	$0.2^{+0.1}_{-0.1}$	$0.4^{+0.7}_{-0.1}$
00015874013	60012.52010	0.94	0.11	2023-03-09 12:22:00	2023-03-09 12:35:52	832	$2.7^{+0.7}_{-0.6}$	$3.6^{+0.9}_{-0.6}$
00015874014	60015.09010	0.16	0.19	2023-03-12 02:01:35	2023-03-12 02:17:53	978	$21.2^{+2.7}_{-2.4}$	$26.8^{+2.9}_{-2.5}$
00015874015	60017.87524	0.40	0.28	2023-03-14 20:51:47	2023-03-14 21:08:53	1025	$29.0^{+3.8}_{-3.3}$	$54.6^{+21.8}_{-9.7}$
00015874016	60019.49996	0.54	0.34	2023-03-16 03:12:00	2023-03-16 20:47:53	1246	$1.1^{+0.6}_{-0.4}$	$1.1^{+0.6}_{-0.4}$
00015874017	60022.43528	0.80	0.43	2023-03-19 00:45:42	2023-03-19 20:07:53	1377	$13.9^{+1.7}_{-1.5}$	$19.9^{+3.2}_{-2.1}$
00015874018	60024.41987	0.97	0.50	2023-03-21 02:03:20	2023-03-21 18:05:52	1311	$42.8^{+3.9}_{-3.5}$	$53.8^{+4.1}_{-3.6}$
00015874019	60026.00975	0.10	0.55	2023-03-23 00:08:12	2023-03-23 00:19:52	700	$20.2^{+3.8}_{-3.1}$	$36.1^{+20.0}_{-7.7}$
00015874020	60035.92511	0.96	0.87	2023-04-01 21:20:25	2023-04-01 23:03:53	700	$6.0^{+1.2}_{-1.0}$	$10.0^{+5.3}_{-2.0}$
00015874021	60038.80610	0.21	0.97	2023-04-04 19:13:40	2023-04-04 19:27:53	852	$3.6^{+0.9}_{-0.7}$	$3.8^{+0.8}_{-0.7}$
00015874022	60040.56001	0.36	0.02	2023-04-06 06:21:57	2023-04-06 20:30:51	945	$17.7^{+2.9}_{-2.4}$	$28.6^{+10.4}_{-4.5}$
00015874023	60042.10699	0.49	0.07	2023-04-08 02:26:13	2023-04-08 02:41:53	940	$2.4^{+0.8}_{-0.6}$	$3.8^{+4.9}_{-1.0}$
00015874024	60045.58485	0.79	0.19	2023-04-11 08:17:29	2023-04-11 19:46:52	1138	$1.0^{+0.3}_{-0.2}$	$1.7^{+1.9}_{-0.4}$
00015874025	60047.20792	0.93	0.24	2023-04-13 04:51:53	2023-04-13 05:06:53	900	$0.6^{+0.4}_{-0.2}$	$0.8^{+3.1}_{-0.3}$
00015874026	60049.24266	0.11	0.30	2023-04-15 05:41:59	2023-04-15 05:56:51	893	$6.8^{+1.7}_{-1.3}$	$7.7^{+1.4}_{-1.1}$
00015874027	60052.28427	0.37	0.40	2023-04-18 06:41:48	2023-04-18 06:56:53	905	–	–
00015874028	60054.60630	0.57	0.48	2023-04-20 14:25:16	2023-04-20 14:40:52	935	–	–
00015874029	60056.85598	0.76	0.55	2023-04-22 20:24:18	2023-04-22 20:40:53	995	$1.7^{+0.4}_{-0.3}$	$2.5^{+1.3}_{-0.5}$
00015874030	60058.03684	0.87	0.59	2023-04-24 00:46:13	2023-04-24 00:59:53	820	$50.8^{+6.2}_{-5.5}$	$63.5^{+6.1}_{-5.5}$
00015874032	60063.07469	0.30	0.75	2023-04-29 01:40:14	2023-04-29 01:54:52	878	$11.5^{+2.4}_{-2.0}$	$15.8^{+4.3}_{-2.3}$
00015874033	60065.28811	0.49	0.83	2023-04-30 22:06:51	2023-05-01 15:42:53	1800	$9.8^{+1.2}_{-1.1}$	$12.7^{+1.4}_{-1.2}$
00015874034	60068.02361	0.73	0.91	2023-05-04 00:28:08	2023-05-04 00:39:52	705	$80.2^{+9.6}_{-8.5}$	$117.9^{+20.3}_{-12.6}$
00015874035	60070.06917	0.90	0.98	2023-05-06 01:32:19	2023-05-06 01:46:52	873	$27.1^{+4.2}_{-3.6}$	$41.2^{+12.3}_{-5.8}$
00015874036	60072.12550	0.08	0.05	2023-05-08 02:51:33	2023-05-08 03:09:53	1101	$28.0^{+4.0}_{-3.5}$	$32.6^{+3.5}_{-3.3}$
00015874037	60075.62487	0.38	0.16	2023-05-11 14:53:43	2023-05-11 15:05:53	730	$1.6^{+0.5}_{-0.4}$	$3.2^{+4.5}_{-0.9}$
00015874038	60077.01463	0.50	0.21	2023-05-13 00:14:15	2023-05-13 00:27:51	767	$0.7^{+1.6}_{-0.5}$	$0.8^{+1.5}_{-0.3}$
00015874039	60088.94118	0.53	0.59	2023-05-24 22:31:42	2023-05-24 22:38:53	431	$1.1^{+1.2}_{-0.6}$	$2.1^{+1.3}_{-0.9}$
00015874040	60091.72302	0.77	0.69	2023-05-27 17:14:23	2023-05-27 17:27:53	810	$0.7^{+0.3}_{-0.2}$	$2.1^{+1.6}_{-1.1}$
00015874041	60093.62734	0.93	0.75	2023-05-29 14:55:49	2023-05-29 15:10:54	905	$7.8^{+1.7}_{-1.4}$	$9.2^{+1.5}_{-1.3}$
00015874042	60095.80837	0.12	0.82	2023-05-31 19:16:13	2023-05-31 19:31:53	940	$32.8^{+3.8}_{-3.4}$	$35.3^{+3.4}_{-3.0}$
00015874043	60097.33644	0.25	0.87	2023-06-02 03:13:04	2023-06-02 12:55:53	1344	$9.0^{+1.1}_{-1.0}$	$12.6^{+1.8}_{-1.2}$
00015874044	60100.11498	0.49	0.96	2023-06-05 01:01:14	2023-06-05 04:29:53	1710	$1.0^{+0.4}_{-0.3}$	$1.2^{+0.8}_{-0.3}$
00015874045	60102.18849	0.67	0.03	2023-06-07 03:40:56	2023-06-07 05:21:53	1387	–	–
00015874046	60104.14462	0.84	0.09	2023-06-09 01:43:38	2023-06-09 05:11:52	1519	$15.6^{+2.1}_{-1.9}$	$18.3^{+1.8}_{-1.7}$
00015874047	60107.02621	0.09	0.18	2023-06-11 22:12:35	2023-06-12 03:02:53	1066	$7.5^{+1.4}_{-1.2}$	$10.2^{+2.4}_{-1.4}$
00015874048	60109.09067	0.27	0.25	2023-06-14 02:03:14	2023-06-14 02:17:54	880	$18.2^{+2.6}_{-2.2}$	$26.3^{+5.1}_{-3.1}$
00015874049	60110.71524	0.41	0.30	2023-06-15 10:02:59	2023-06-16 00:16:53	875	$3.0^{+0.8}_{-0.6}$	$5.5^{+6.1}_{-1.4}$
00015874050	60114.32445	0.72	0.42	2023-06-19 07:39:32	2023-06-19 07:54:52	920	$3.0^{+0.7}_{-0.5}$	$5.8^{+5.4}_{-1.6}$
00015874051	60116.23916	0.88	0.48	2023-06-21 05:34:52	2023-06-21 05:53:53	1141	$22.2^{+3.7}_{-3.2}$	$25.0^{+3.3}_{-2.9}$
00015874052	60118.93825	0.12	0.57	2023-06-23 22:23:15	2023-06-23 22:38:53	938	$1.1^{+0.4}_{-0.3}$	$2.4^{+5.5}_{-0.8}$
00015874053	60121.26255	0.32	0.65	2023-06-26 06:10:15	2023-06-26 06:25:53	938	–	–
00015874054	60123.87309	0.54	0.73	2023-06-28 20:07:38	2023-06-28 21:46:52	1118	–	–
00015874055	60125.15684	0.65	0.77	2023-06-30 03:38:49	2023-06-30 03:52:52	842	–	–

Table A1. Observation log for 2S 0114+650, continued.

ObsID	MJD	Orbital[a] Phase	Super-o.[b] Phase	Start time (UT) (yyyy-mm-dd hh:mm:ss)	End time (UT) (yyyy-mm-dd hh:mm:ss)	Exposure (s)	Flux[c] (erg cm^{-2} s^{-1})	Flux[d] (erg cm^{-2} s^{-1})
00015874056	60127.59959	0.86	0.85	2023-07-02 14:14:56	2023-07-02 14:31:52	1015	$2.1^{+0.6}_{-0.5}$	$2.8^{+0.7}_{-0.5}$
00015874057	60129.54923	0.03	0.92	2023-07-04 01:13:52	2023-07-05 01:07:54	1101	$1.3^{+0.4}_{-0.3}$	$1.7^{+0.6}_{-0.3}$
00015874058	60141.69904	0.08	0.31	2023-07-16 16:38:20	2023-07-16 16:54:53	993	–	–
00015874059	60144.53360	0.32	0.40	2023-07-19 12:40:54	2023-07-19 12:55:51	898	$29.4^{+4.1}_{-3.6}$	$39.2^{+5.5}_{-4.1}$
00015874060	60146.46352	0.49	0.47	2023-07-21 01:33:04	2023-07-21 20:41:52	1038	$6.5^{+1.7}_{-1.4}$	$8.3^{+2.8}_{-1.5}$
00015874061	60148.17633	0.64	0.52	2023-07-23 02:33:57	2023-07-23 05:53:52	1249	$4.4^{+0.9}_{-0.7}$	$7.9^{+6.9}_{-1.8}$
00015874062	60150.41982	0.83	0.59	2023-07-25 08:33:12	2023-07-25 11:35:52	1111	$20.3^{+2.4}_{-2.1}$	$26.4^{+2.8}_{-2.3}$
00015874063	60153.92619	0.13	0.71	2023-07-28 22:05:32	2023-07-28 22:21:52	980	$8.2^{+1.6}_{-1.3}$	$13.9^{+7.9}_{-2.8}$
00015874064	60155.90796	0.30	0.77	2023-07-30 21:40:02	2023-07-30 21:54:52	890	–	–
00015874065	60157.35743	0.43	0.82	2023-08-01 05:28:30	2023-08-01 11:40:52	955	–	–
00015874066	60160.59398	0.71	0.92	2023-08-04 14:07:46	2023-08-04 14:22:54	908	$1.8^{+0.5}_{-0.4}$	$3.5^{+6.9}_{-1.1}$
00015874067	60162.60713	0.88	0.99	2023-08-06 13:48:38	2023-08-06 15:19:52	1178	$4.2^{+0.9}_{-0.7}$	$5.9^{+1.6}_{-0.9}$
00015874068	60164.22094	0.02	0.04	2023-08-08 05:10:41	2023-08-08 05:25:54	895	$3.9^{+0.7}_{-0.6}$	$6.2^{+2.2}_{-1.1}$
00015874069	60168.04810	0.35	0.17	2023-08-11 12:22:37	2023-08-12 13:55:53	1108	$2.9^{+0.6}_{-0.5}$	$4.4^{+2.2}_{-0.8}$
00015874070	60170.00772	0.52	0.23	2023-08-13 17:00:19	2023-08-14 07:21:53	1364	$0.5^{+0.3}_{-0.2}$	$8.5^{+11.4}_{-7.6}$
00015874071	60171.55790	0.65	0.28	2023-08-15 11:46:51	2023-08-15 14:59:54	1046	$13.9^{+2.3}_{-1.9}$	$35.1^{+12.8}_{-10.6}$
00015874072	60173.20319	0.80	0.33	2023-08-17 04:42:19	2023-08-17 05:02:52	1234	$17.0^{+2.7}_{-2.3}$	$22.9^{+4.2}_{-2.7}$
00015874073	60176.64572	0.09	0.45	2023-08-20 15:22:47	2023-08-20 15:36:52	845	$1.4^{+0.8}_{-0.5}$	$1.5^{+0.6}_{-0.4}$
00015874074	60178.62604	0.26	0.51	2023-08-22 14:54:07	2023-08-22 15:08:52	885	$2.6^{+0.8}_{-0.6}$	$3.2^{+1.0}_{-0.6}$
00015874075	60180.27359	0.40	0.56	2023-08-24 06:27:03	2023-08-24 06:40:53	830	$3.9^{+1.0}_{-0.8}$	$4.9^{+1.1}_{-0.8}$

Notes: [a] Phase zero for the orbital period is the time of periastron passage at MJD 51824.8 (Grundstrom et al. 2007). [b] Phase zero for the superorbital period is the minimum of the folded light curve at MJD 53488 (Farrell et al. 2008). [c] Observed flux in the 0.3–10 keV energy band in units of $\times 10^{-11}$ erg cm^{-2} s^{-1}. When no value is provided, the observation yielded insufficient counts to perform spectral analysis. [d] Unabsorbed flux in the 0.3–10 keV energy band in units of $\times 10^{-11}$ erg cm^{-2} s^{-1}.

APPENDIX B: ADDITIONAL MATERIAL

As reported in Sect. 2.1, the X-ray light curves of 2S 0114+650 show variability on different timescales, namely, the spin period $P_{spin} \sim 9800$ s, the orbital period P_{orb}=11.5983 d, and the superorbital period P_{sup}=30.76 d. In order to clarify the effects of binning of the data on these different timescales on our results we also calculated the spin phase for each observation (Table A1). We note that the typical exposure time of our observations is generally a factor of 10 shorter than P_{spin}, so we addressed the possibility that in each orbital phase bin the spin phases would not be equally represented.

Figure B1 (left) shows as grey empty squares where our sample of observations occur in the orbital phase and as grey downward-pointing empty triangles where they occur in spin phase (see, e.g. the first two rows). For each orbital phase bin (filled squares: red for the first bin, orange for the second bin, green for the third and so on) on the first row, we report as filled triangles the matching observations in spin phase in the second row (with the same colour). As can be observed, the spin phases, albeit being a small number, are not preferentially clustered. Therefore we can argue that, within the limits of our discrete sampling of the light curve of 2S 0114+650, we are not introducing strong biases due to the distribution of our observations in spin phase in each orbital phase bin.

Similarly, to address the possibility that in each superorbital phase bin the orbital phases would not be equally represented, Figure B1 (right) shows as grey upward-pointing empty triangles where our sample of observations occur in the superorbital phase, as grey empty squares where our sample of observations occur in the orbital phase and as grey downward-pointing empty triangles where they occur in spin phase (e.g., the first three rows). For each superorbital phase bin (filled triangles with the same colour scheme) on the first row, we report as filled symbols the matching observations in orbital phase in the second row and spin phase in the third row (with the same colour). Once more, we can argue that we are not introducing strong biases due to the distribution of our observations in orbital phase in each superorbital orbital phase bin.

We finally consider the other sources which data we reported in Table 1. In the case of IGR J16418−4532 and IGR J16493−4348 the pulsation timescale is in the order of ∼ 1 ks, comparable with the typical XRT exposure. The XRT data thus sample automatically all spin phases in each observation. For IGR J16479−4514, no pulsations were ever detected and thus no such investigation is possible at this time.

This paper has been typeset from a TEX/LATEX file prepared by the author.

Table A2. Observation log for IGR J16418−4532. Observing sequence, date (MJD of the middle of the observation), superorbital phase, start and end times (UTC), XRT exposure time, and 0.3–10 keV observed and unabsorbed flux, and references.

ObsID	MJD	Phase	Start time (UT) (yyyy-mm-dd hh:mm:ss)	End time (UT) (yyyy-mm-dd hh:mm:ss)	Exposure (s)	Flux[a] (erg cm^{-2} s^{-1})	Flux[b] (erg cm^{-2} s^{-1})	Ref.
00031929001	55610.11915	0.90	2011-02-18 01:59:42	2011-02-18 03:43:25	1953	$16.4^{+2.3}_{-2.0}$	$30.0^{+14.4}_{-5.6}$	1
00031929002	55624.10599	0.85	2011-03-04 00:03:18	2011-03-04 05:01:56	2021	$10.1^{+1.4}_{-1.2}$	$13.5^{+1.8}_{-1.4}$	
00031929003	55755.51071	0.77	2011-07-13 09:46:54	2011-07-13 14:43:56	4756	$6.9^{+0.6}_{-0.5}$	$10.0^{+1.0}_{-0.8}$	
00031929004	55756.67068	0.85	2011-07-14 12:39:38	2011-07-14 19:31:55	4832	$0.5^{+0.3}_{-0.2}$	$4.4^{+31.9}_{-3.5}$	
00031929005	55757.61961	0.91	2011-07-15 06:42:49	2011-07-15 23:01:56	1081	$1.4^{+0.8}_{-0.5}$	$1.8^{+8.0}_{-0.3}$	
00031929006	55758.69515	0.98	2011-07-16 10:15:04	2011-07-16 23:06:57	396	$7.1^{+3.7}_{-2.4}$	$9.5^{+46.6}_{-2.5}$	
00031929007	55761.52284	0.18	2011-07-19 01:52:40	2011-07-19 23:19:56	2673	$7.2^{+0.9}_{-0.8}$	$9.8^{+1.3}_{-1.0}$	
00032037001	55760.96527	0.14	2011-07-18 21:28:27	2011-07-19 00:51:30	1941	–	–	
00032037002	55762.43113	0.24	2011-07-20 05:18:41	2011-07-20 15:22:57	3503	$5.6^{+0.6}_{-0.5}$	$8.9^{+1.7}_{-1.0}$	
00032037003	55763.53270	0.31	2011-07-21 10:06:17	2011-07-21 15:27:53	3779	$1.9^{+0.3}_{-0.3}$	$2.7^{+0.7}_{-0.4}$	
00032037004	55764.70995	0.39	2011-07-22 15:19:42	2011-07-22 18:44:56	2818	–	–	
00032037005	55765.56675	0.45	2011-07-23 11:48:18	2011-07-23 15:23:55	4145	$3.7^{+0.4}_{-0.4}$	$5.7^{+1.2}_{-0.7}$	
00032037006	55771.74599	0.87	2011-07-29 12:13:29	2011-07-29 23:34:56	4669	–	–	
00032037007	55772.24797	0.90	2011-07-30 01:01:29	2011-07-30 10:52:57	5082	$0.5^{+0.1}_{-0.1}$	$0.8^{+0.6}_{-0.2}$	
00523489000	56081.80123	0.92	2012-06-03 18:16:39	2012-06-03 20:10:52	2771	$8.4^{+1.0}_{-0.9}$	$66.2^{+192.8}_{-35.4}$	2, 3, 4
00523489001	56082.65221	0.98	2012-06-04 13:06:06	2012-06-04 18:12:15	3280	$4.2^{+0.6}_{-0.6}$	$7.0^{+3.5}_{-1.2}$	
00552677000	56384.54853	0.47	2013-04-02 12:16:51	2013-04-02 14:02:54	2191	$35.5^{+3.0}_{-2.7}$	$55.5^{+7.5}_{-5.0}$	4
00571067000	56552.67883	0.89	2013-09-17 16:08:16	2013-09-17 16:26:44	1108	$3.8^{+0.9}_{-0.7}$	$7.5^{+20.5}_{-2.4}$	4
00032037008	56553.43540	0.94	2013-09-18 09:21:35	2013-09-18 11:32:22	975	–	–	
00032037009	56554.24883	0.99	2013-09-19 00:18:42	2013-09-19 11:37:54	973	$7.9^{+1.5}_{-1.3}$	$11.7^{+3.9}_{-1.7}$	
00032037010	56555.07223	0.05	2013-09-20 01:36:05	2013-09-20 01:51:55	950	$9.6^{+2.4}_{-1.9}$	$17.1^{+20.0}_{-4.3}$	
00032037011	56556.26644	0.13	2013-09-21 06:15:24	2013-09-21 06:31:55	990	$7.4^{+1.5}_{-1.2}$	$16.6^{+18.5}_{-4.7}$	
00032037012	56557.61314	0.22	2013-09-22 14:34:56	2013-09-22 14:50:54	958	$0.7^{+0.4}_{-0.3}$	$1.4^{+15.8}_{-0.6}$	
00032037013	56558.40401	0.28	2013-09-23 09:33:38	2013-09-23 09:49:53	975	$0.7^{+0.9}_{-0.4}$	$0.8^{+1.0}_{-0.3}$	
00032037014	56559.68368	0.36	2013-09-24 16:16:06	2013-09-24 16:32:53	1008	$0.6^{+0.3}_{-0.2}$	$1.2^{+7.2}_{-0.5}$	
00032037015	56907.15963	0.95	2014-09-07 03:41:49	2014-09-07 03:57:54	965	$4.7^{+1.2}_{-1.0}$	$6.0^{+2.7}_{-1.1}$	5
00032037016	56910.69873	0.19	2014-09-10 13:16:25	2014-09-10 20:15:54	1088	$6.8^{+1.7}_{-1.4}$	$10.9^{+9.0}_{-2.2}$	
00032037017	56914.95235	0.48	2014-09-14 22:43:50	2014-09-14 22:58:55	905	$1.6^{+0.7}_{-0.5}$	$2.0^{+1.3}_{-0.5}$	
00032037018	56917.09152	0.63	2014-09-17 02:03:38	2014-09-17 02:19:55	978	–	–	
00032037019	56921.94654	0.96	2014-09-21 22:35:06	2014-09-21 22:50:54	948	$2.3^{+0.9}_{-0.6}$	$3.3^{+3.3}_{-0.8}$	
00032037020	56924.61884	0.14	2014-09-24 14:48:50	2014-09-24 14:53:25	276	$9.7^{+3.6}_{-2.5}$	$19.1^{+66.2}_{-6.7}$	
00032037021	56928.13989	0.38	2014-09-28 03:20:40	2014-09-28 03:22:11	90	–	–	
00032037022	56931.14320	0.58	2014-10-01 03:18:28	2014-10-01 03:33:55	928	–	–	
00032037023	56935.01289	0.84	2014-10-05 00:10:10	2014-10-05 00:26:56	1005	–	–	
00032037024	56938.21281	0.06	2014-10-08 04:58:59	2014-10-08 05:13:54	895	–	–	
00032037025	56942.94418	0.38	2014-10-12 22:29:20	2014-10-12 22:49:54	1234	$9.7^{+1.8}_{-1.5}$	$15.0^{+6.6}_{-2.3}$	
00032037026	56945.71201	0.57	2014-10-15 14:43:38	2014-10-15 19:26:56	1031	–	–	
00032037027	56949.53568	0.83	2014-10-19 09:40:03	2014-10-19 16:02:54	1221	–	–	
00032037029	56955.07324	0.21	2014-10-25 01:34:01	2014-10-25 01:56:55	1374	$1.6^{+0.7}_{-0.5}$	$4.1^{+29.9}_{-1.7}$	
00032037030	57040.49987	0.00	2015-01-18 11:51:43	2015-01-18 12:07:54	970	$9.3^{+1.7}_{-1.4}$	$16.3^{+8.3}_{-3.1}$	
00032037031	57043.16719	0.19	2015-01-21 03:52:36	2015-01-21 04:08:54	978	–	–	
00032037032	57047.68975	0.49	2015-01-25 16:25:33	2015-01-25 16:40:55	923	$8.0^{+1.5}_{-1.3}$	$11.1^{+2.4}_{-1.4}$	
00032037033	57050.95139	0.71	2015-01-28 22:42:06	2015-01-28 22:57:54	948	–	–	
00032037034	57054.02305	0.92	2015-02-01 00:24:29	2015-02-01 00:41:54	1046	–	–	
00639199000	57139.60458	0.73	2015-04-27 14:25:53	2015-04-27 14:35:17	564	$38.5^{+7.5}_{-6.4}$	$50.0^{+9.4}_{-6.7}$	4
00032037036	57141.19595	0.84	2015-04-29 04:34:23	2015-04-29 04:49:56	933	$3.4^{+0.7}_{-0.6}$	$7.0^{+6.7}_{-1.8}$	
00032037037	57142.98612	0.96	2015-04-30 23:33:21	2015-04-30 23:46:39	797	$1.1^{+0.5}_{-0.3}$	$16.9^{+179.5}_{-14.9}$	
00032037038	57143.24946	0.98	2015-05-01 01:10:31	2015-05-01 10:47:55	707	$3.1^{+1.2}_{-0.8}$	$7.0^{+81.0}_{-2.8}$	4
00032037039	57144.85102	0.09	2015-05-02 20:18:02	2015-05-02 20:32:54	893	$4.3^{+1.3}_{-1.0}$	$6.1^{+3.2}_{-1.1}$	
01073821000	59475.38643	0.31	2021-09-18 09:08:42	2021-09-18 09:24:13	930	$30.5^{+3.9}_{-3.5}$	$39.3^{+4.4}_{-3.7}$	6, 4
01073821001	59475.48760	0.31	2021-09-18 10:43:44	2021-09-18 12:40:33	2951	$4.0^{+0.6}_{-0.5}$	$6.3^{+1.6}_{-0.9}$	

Table A2. Observation log for IGR J16418−4532. Continued.

ObsID	MJD	Phase	Start time (UT) (yyyy-mm-dd hh:mm:ss)	End time (UT) (yyyy-mm-dd hh:mm:ss)	Exposure (s)	Flux[a] (erg cm^{-2} s^{-1})	Flux[b] (erg cm^{-2} s^{-1})	Ref.
00043105001	55739.22181	0.66	2011-06-27 05:14:53	2011-06-27 05:23:55	542	$3.5^{+1.8}_{-1.2}$	$4.6^{+4.1}_{-1.2}$	7
00081650001	57291.94305	0.07	2015-09-26 21:43:06	2015-09-26 23:32:53	1891	$6.2^{+1.0}_{-0.9}$	$7.8^{+1.1}_{-0.9}$	
00088748001	58393.93698	0.89	2018-10-02 21:32:47	2018-10-02 23:25:52	1800	$2.0^{+0.4}_{-0.4}$	$2.6^{+0.8}_{-0.4}$	8
00088748002	58401.90480	0.43	2018-10-10 20:45:56	2018-10-10 22:39:52	1790	$4.4^{+0.7}_{-0.6}$	$6.0^{+1.3}_{-0.8}$	

Notes: [a] Observed flux in the 0.3–10 keV energy band in units of $\times10^{-11}$ erg cm^{-2} s^{-1}. When no value is provided, the observation yielded insufficient counts to perform spectral analysis. [b] Unabsorbed flux in the 0.3–10 keV energy band in units of $\times10^{-11}$ erg cm^{-2} s^{-1}.

(1) Monitoring campaign in Romano et al. (2012a); (2) Romano et al. (2012b); (3) Romano et al. (2013); (4) Outbursts and followups in Romano et al. (2023); (5) Monitoring campaign, this work. (6) Sbarufatti et al. (2021); (7) Serendipitous observations, this work; (8) Islam et al. (2023).

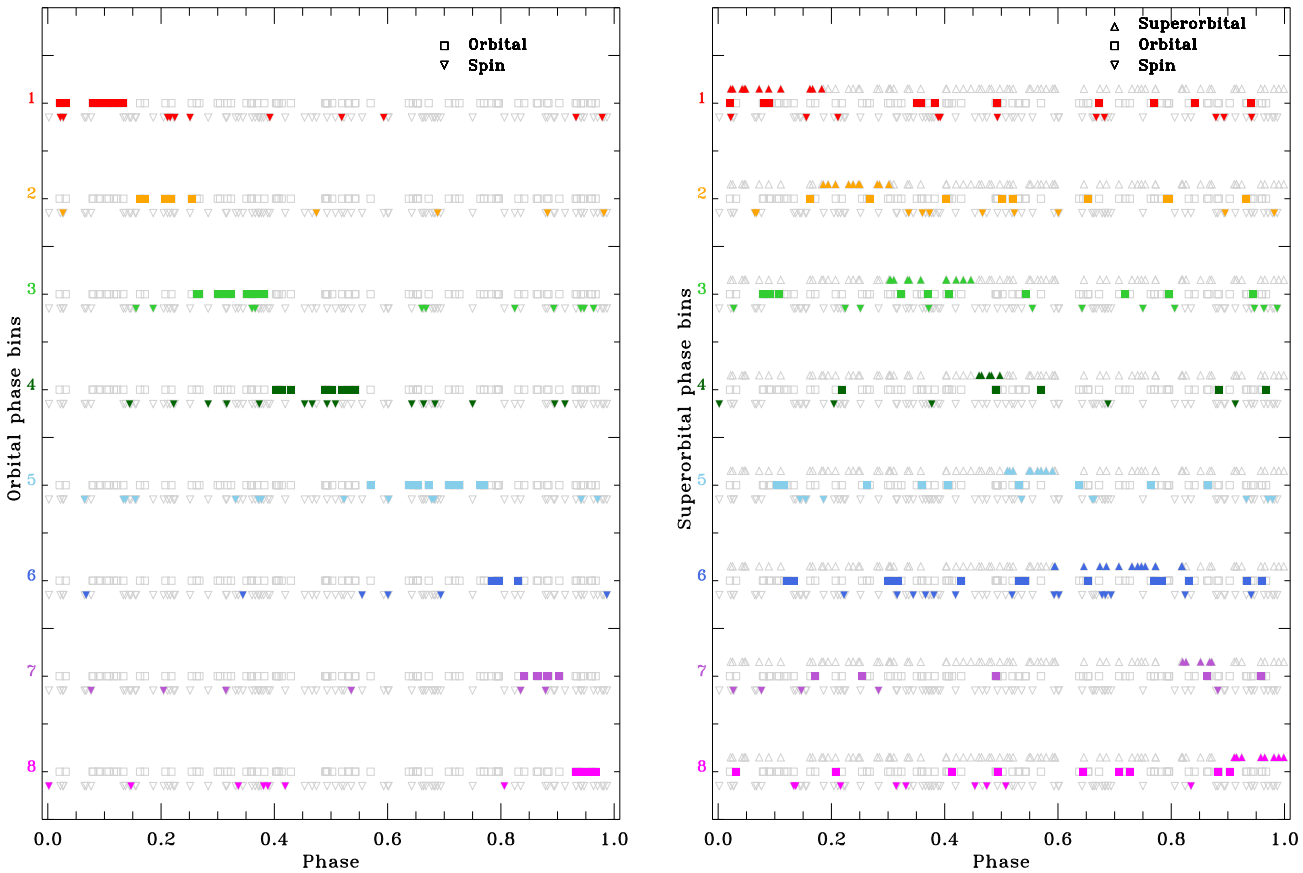

Figure B1. *Left:* Distribution of the observations collected on 2S 0114+650 (on the x axis) in orbital phase (grey empty squares), and spin phase (grey empty downward-pointing triangles) as a function of orbital phase bin (on the y axis). The observations for each orbital phase bin are shown in different colours as filled symbols and offset for clarity. *Right:* Distribution of the observations collected on 2S 0114+650 (on the x axis) in superorbital phase (grey empty upward-pointing triangles), orbital phase (grey empty squares), and spin phase (grey empty downward-pointing triangles) as a function of superorbital phase bin (on the y axis). The observations for each superorbital phase bin are shown in different colours as filled symbols and offset for clarity.

Table A3. Observation log for IGR J16479−4514. Observing sequence, date (MJD of the middle of the observation), superorbital phase, start and end times (UTC), XRT exposure time, and 0.3–10 keV observed and unabsorbed flux.

ObsID	MJD	Phase	Start time (UT) (yyyy-mm-dd hh:mm:ss)	End time (UT) (yyyy-mm-dd hh:mm:ss)	Exposure (s)	Flux (erg cm^{-2} s^{-1})	Flux (erg cm^{-2} s^{-1})
00030296006	54484.96264	0.81	2008-01-19 22:58:28	2008-01-19 23:13:58	928	$12.5^{+3.3}_{-2.6}$	$15.9^{+3.6}_{-2.6}$
00030296007	54487.84512	0.05	2008-01-22 20:07:57	2008-01-22 20:25:58	1081	$2.5^{+0.6}_{-0.5}$	$4.6^{+5.7}_{-1.2}$
00030296008	54491.79550	0.38	2008-01-26 18:56:04	2008-01-26 19:14:57	1133	$1.4^{+0.6}_{-0.4}$	$2.2^{+3.2}_{-0.5}$
00030296009	54494.34173	0.60	2008-01-29 08:03:13	2008-01-29 08:20:56	1063	$0.4^{+0.4}_{-0.2}$	$0.5^{+0.6}_{-0.2}$
00030296010	54501.37081	0.19	2008-02-05 00:48:59	2008-02-05 16:58:56	3056	$1.8^{+0.3}_{-0.2}$	$8.3^{+21.8}_{-4.1}$
00030296011	54505.89050	0.57	2008-02-09 18:53:39	2008-02-09 23:50:58	2751	$4.2^{+0.6}_{-0.5}$	$5.2^{+0.5}_{-0.5}$
00030296012	54506.12279	0.59	2008-02-10 01:16:40	2008-02-10 04:36:58	873	$1.8^{+0.5}_{-0.4}$	$4.3^{+12.2}_{-1.6}$
00030296013	54511.37989	0.03	2008-02-15 08:12:38	2008-02-15 10:01:25	1254	$1.2^{+0.3}_{-0.2}$	–
00030296014	54514.35488	0.28	2008-02-18 06:49:05	2008-02-18 10:12:57	1151	$4.4^{+1.0}_{-0.8}$	$22.6^{+240.6}_{-13.7}$
00030296015	54516.02799	0.42	2008-02-20 00:33:38	2008-02-20 00:46:58	800	$0.5^{+0.5}_{-0.2}$	$1.1^{+5.0}_{-0.5}$
00030296016	54519.94461	0.75	2008-02-23 21:44:31	2008-02-23 23:35:57	1667	$0.9^{+0.3}_{-0.2}$	$1.8^{+18.3}_{-0.7}$
00030296017	54522.98995	0.01	2008-02-26 23:38:06	2008-02-26 23:52:56	890	–	–
00030296018	54526.99264	0.35	2008-03-01 23:38:51	2008-03-01 23:59:59	1266	–	–
00030296019	54528.14534	0.44	2008-03-03 01:50:45	2008-03-03 05:07:56	1076	–	–
00030296020	54531.05549	0.69	2008-03-06 00:26:49	2008-03-06 02:12:58	1101	–	–
00030296021	54535.44502	0.06	2008-03-10 09:05:42	2008-03-10 12:15:56	1261	$27.2^{+3.6}_{-3.2}$	$38.7^{+7.2}_{-4.4}$
00030296022	54536.90404	0.18	2008-03-11 20:00:41	2008-03-11 23:22:56	2986	$0.1^{+0.1}_{-0.0}$	$1.7^{+20.1}_{-1.6}$
00030296023	54537.88839	0.26	2008-03-12 18:46:44	2008-03-12 23:51:49	2776	$5.6^{+0.7}_{-0.6}$	$10.5^{+3.9}_{-1.7}$
00030296024	54538.18389	0.29	2008-03-13 04:14:40	2008-03-13 04:34:56	1214	$2.7^{+0.7}_{-0.5}$	$6.0^{+10.6}_{-1.9}$
00030296025	54540.19923	0.46	2008-03-15 04:37:49	2008-03-15 04:55:57	1088	–	–
00030296026	54541.33765	0.55	2008-03-16 07:56:54	2008-03-16 08:15:30	1116	$4.8^{+0.9}_{-0.8}$	$7.7^{+3.4}_{-1.3}$
00030296027	54542.31110	0.64	2008-03-17 06:34:08	2008-03-17 08:21:48	1216	$0.3^{+0.4}_{-0.2}$	$0.5^{+2.9}_{-0.2}$
00030296028	54543.47703	0.73	2008-03-18 06:31:54	2008-03-18 16:21:56	2342	$0.3^{+0.2}_{-0.1}$	$0.3^{+0.2}_{-0.1}$
00030296029	54544.82184	0.85	2008-03-19 19:38:56	2008-03-19 19:47:57	542	$0.8^{+0.6}_{-0.3}$	$1.7^{+24.1}_{-0.8}$
00306829000	54544.99873	0.86	2008-03-19 23:55:27	2008-03-20 00:00:53	326	$8.7^{+2.9}_{-2.0}$	$44.8^{+203.9}_{-27.1}$
00030296030	54546.12308	0.96	2008-03-21 02:05:29	2008-03-21 03:48:58	835	$1.6^{+1.5}_{-0.7}$	$6.5^{+7.8}_{-4.5}$
00030296031	54546.92654	0.02	2008-03-21 21:22:28	2008-03-21 23:05:57	835	–	–
00030296032	54548.22937	0.13	2008-03-23 05:25:03	2008-03-23 05:35:30	627	$0.3^{+0.4}_{-0.2}$	$0.6^{+2.4}_{-0.3}$
00030296033	54549.25965	0.22	2008-03-24 05:36:51	2008-03-24 06:50:56	1041	$3.9^{+0.9}_{-0.7}$	$5.5^{+1.9}_{-0.9}$
00030296034	54566.73909	0.69	2008-04-10 15:17:37	2008-04-10 20:10:57	905	–	–
00030296035	54588.93000	0.56	2008-05-02 22:12:26	2008-05-02 22:25:56	810	$14.6^{+3.2}_{-2.6}$	$21.4^{+9.2}_{-3.7}$
00030296036	54592.86247	0.89	2008-05-06 20:40:14	2008-05-06 20:43:39	206	–	–
00030296037	54596.41810	0.19	2008-05-10 09:53:10	2008-05-10 10:10:56	1066	$3.0^{+0.7}_{-0.6}$	$10.4^{+39.2}_{-4.9}$
00030296038	54600.36325	0.52	2008-05-14 08:33:12	2008-05-14 08:52:58	1186	–	–
00030296039	54608.90984	0.24	2008-05-22 20:54:24	2008-05-22 22:45:56	2374	$0.6^{+0.3}_{-0.2}$	$1.1^{+5.2}_{-0.3}$
00030296040	54612.88702	0.58	2008-05-26 21:05:40	2008-05-26 21:28:57	1397	$2.8^{+0.6}_{-0.5}$	$4.0^{+1.6}_{-0.7}$
00030296041	54617.05938	0.93	2008-05-30 08:40:01	2008-05-31 18:10:58	995	$2.0^{+1.4}_{-0.8}$	$3.9^{+41.4}_{-1.5}$
00030296042	54620.85094	0.25	2008-06-03 20:15:44	2008-06-03 20:34:57	1153	$1.8^{+0.7}_{-0.5}$	$2.0^{+0.7}_{-0.5}$
00030296043	54624.67212	0.57	2008-06-07 16:05:45	2008-06-07 16:09:56	251	$12.8^{+3.1}_{-2.5}$	$24.0^{+25.8}_{-6.1}$
00030296044	54628.38194	0.88	2008-06-11 08:22:02	2008-06-11 09:57:56	736	–	–
00030296046	54636.74855	0.58	2008-06-19 17:03:51	2008-06-19 18:51:58	1512	–	–
00030296047	54640.38837	0.89	2008-06-23 09:12:34	2008-06-23 09:25:56	802	$1.6^{+0.9}_{-0.5}$	$32.6^{+189.2}_{-28.9}$
00030296048	54645.11642	0.29	2008-06-28 00:35:19	2008-06-28 04:59:57	970	$2.4^{+0.6}_{-0.5}$	$3.7^{+2.6}_{-0.8}$
00030296049	54648.22275	0.55	2008-07-01 05:12:34	2008-07-01 05:28:57	983	$2.5^{+0.7}_{-0.5}$	$3.9^{+3.3}_{-0.9}$
00030296050	54652.58477	0.92	2008-07-05 13:53:11	2008-07-05 14:10:57	1066	$0.7^{+0.5}_{-0.3}$	$0.7^{+0.5}_{-0.3}$
00030296052	54660.44651	0.58	2008-07-13 09:51:01	2008-07-13 11:34:56	948	$2.2^{+0.6}_{-0.5}$	$5.3^{+13.4}_{-1.9}$
00030296053	54664.56157	0.93	2008-07-17 13:26:34	2008-07-17 13:30:44	251	–	–
00030296055	54668.09847	0.22	2008-07-21 02:13:37	2008-07-21 02:29:57	980	$2.2^{+0.7}_{-0.5}$	$2.7^{+1.0}_{-0.5}$
00030296056	54672.12657	0.56	2008-07-25 02:53:34	2008-07-25 03:10:57	1043	$7.0^{+1.8}_{-1.4}$	–
00030296057	54676.40988	0.92	2008-07-29 09:41:29	2008-07-29 09:58:57	1020	–	–
00030296058	54680.57905	0.27	2008-08-02 13:00:42	2008-08-02 14:46:58	933	$7.9^{+1.6}_{-1.3}$	$15.0^{+11.7}_{-3.3}$
00030296059	54684.09551	0.57	2008-08-06 02:09:08	2008-08-06 02:25:56	1008	$28.0^{+4.5}_{-3.9}$	$40.9^{+9.4}_{-5.3}$
00030296060	54688.04478	0.90	2008-08-10 00:57:00	2008-08-10 01:11:57	898	$4.0^{+1.6}_{-1.1}$	$5.5^{+5.5}_{-1.3}$
00030296061	54692.80424	0.30	2008-08-14 19:10:16	2008-08-14 19:25:56	940	–	–
00030296062	54696.48327	0.61	2008-08-18 11:27:53	2008-08-18 11:43:56	963	–	–
00030296063	54700.62840	0.96	2008-08-22 07:01:50	2008-08-22 23:07:57	755	–	–

Table A3. Observation log for IGR J16479−4514. Continued.

ObsID	MJD	Phase	Start time (UT) (yyyy-mm-dd hh:mm:ss)	End time (UT) (yyyy-mm-dd hh:mm:ss)	Exposure (s)	Flux[a] (erg cm^{-2} s^{-1})	Flux[b] (erg cm^{-2} s^{-1})
00030296065	54708.09900	0.59	2008-08-30 01:29:10	2008-08-30 03:15:56	1236	$5.5^{+1.2}_{-1.0}$	$7.0^{+1.2}_{-1.0}$
00030296066	54720.97606	0.67	2008-09-11 23:18:06	2008-09-11 23:32:56	890	$1.0^{+0.5}_{-0.3}$	$8.7^{+84.4}_{-6.9}$
00030296067	54724.32964	0.96	2008-09-15 07:46:25	2008-09-15 08:02:56	990	$0.7^{+0.3}_{-0.2}$	$3.6^{+37.8}_{-2.4}$
00030296070	54736.24306	0.96	2008-09-27 05:41:07	2008-09-27 05:58:55	1066	–	–
00030296071	54740.66567	0.33	2008-10-01 15:49:11	2008-10-01 16:07:57	1126	$0.4^{+0.5}_{-0.2}$	$16.0^{+173.0}_{-15.4}$
00030296073	54751.97333	0.28	2008-10-12 23:14:15	2008-10-12 23:28:55	880	$1.2^{+0.5}_{-0.4}$	$4.4^{+13.6}_{-2.5}$
00030296074	54756.09479	0.63	2008-10-17 01:27:07	2008-10-17 03:05:57	466	–	–
00030296075	54760.20390	0.98	2008-10-21 04:46:15	2008-10-21 05:00:57	883	$1.8^{+0.7}_{-0.5}$	$2.4^{+1.8}_{-0.5}$
00030296076	54764.95512	0.38	2008-10-25 22:48:38	2008-10-25 23:02:05	807	$9.4^{+1.9}_{-1.5}$	$15.7^{+8.9}_{-3.1}$
00341452000	54860.32175	0.40	2009-01-29 06:47:34	2009-01-29 08:39:03	2660	$19.2^{+2.3}_{-2.0}$	$27.7^{+4.6}_{-2.9}$
00030296077	54860.80421	0.44	2009-01-29 15:59:43	2009-01-29 22:36:23	5927	$3.9^{+0.4}_{-0.3}$	$6.2^{+1.1}_{-0.7}$
00030296078	54861.25266	0.48	2009-01-30 05:05:44	2009-01-30 07:01:55	2482	$4.0^{+0.6}_{-0.5}$	$6.7^{+2.3}_{-1.0}$
00030296079	54862.05578	0.55	2009-01-31 00:23:44	2009-01-31 02:17:57	1366	$0.6^{+0.3}_{-0.2}$	$1.0^{+4.5}_{-0.3}$
00030296080	54863.86170	0.70	2009-02-01 19:50:45	2009-02-01 21:30:56	2043	$0.8^{+0.3}_{-0.2}$	$0.9^{+0.3}_{-0.2}$
00030296081	54864.42608	0.75	2009-02-02 08:46:11	2009-02-02 11:40:56	1903	$0.4^{+0.3}_{-0.1}$	$1.1^{+6.2}_{-0.6}$
00030296082	54865.83880	0.87	2009-02-03 18:25:47	2009-02-03 21:49:57	1236	–	–
00030296083	54866.10478	0.89	2009-02-04 00:51:49	2009-02-04 04:09:55	1409	–	–
00030296084	54867.10934	0.98	2009-02-05 02:24:24	2009-02-05 02:50:29	1507	$2.0^{+0.6}_{-0.5}$	$3.1^{+3.6}_{-0.7}$
00030296085	54868.11879	0.06	2009-02-06 01:13:11	2009-02-06 04:28:56	486	$2.3^{+1.3}_{-0.8}$	$2.7^{+1.1}_{-0.8}$
00030296087	54870.85766	0.29	2009-02-08 18:54:07	2009-02-08 22:15:56	1620	$22.7^{+2.6}_{-2.3}$	$32.9^{+4.9}_{-3.2}$
00030296088	54872.23515	0.41	2009-02-10 03:10:17	2009-02-10 08:06:56	1565	–	–
00030296089	54873.80090	0.54	2009-02-11 15:47:38	2009-02-11 22:38:56	2247	$7.9^{+1.1}_{-0.9}$	$17.5^{+12.1}_{-4.1}$
00030296090	54874.97612	0.64	2009-02-12 22:30:17	2009-02-13 00:20:55	1695	–	–
00030296091	54875.24659	0.66	2009-02-13 05:04:17	2009-02-13 06:45:53	1314	–	–
00030296092	54876.31004	0.75	2009-02-14 06:34:00	2009-02-14 08:18:55	1271	$2.7^{+0.8}_{-0.6}$	$3.0^{+0.7}_{-0.5}$
00030296093	54877.14570	0.82	2009-02-15 03:19:40	2009-02-15 03:39:56	1216	–	–
00030296094	54878.38930	0.93	2009-02-16 08:26:28	2009-02-16 10:14:41	1126	$2.5^{+0.7}_{-0.5}$	$6.2^{+21.6}_{-2.4}$
00030296095	54879.02144	0.98	2009-02-17 00:22:54	2009-02-17 00:38:49	955	–	–
00030296096	54881.92902	0.22	2009-02-19 21:23:38	2009-02-19 23:11:55	1201	$4.6^{+1.0}_{-0.8}$	$7.1^{+3.6}_{-1.3}$
00030296097	54885.67519	0.54	2009-02-23 15:15:36	2009-02-23 17:08:57	1933	–	–
00030296098	54888.89594	0.81	2009-02-26 20:38:21	2009-02-26 22:21:57	910	–	–
00030296099	54891.10343	1.00	2009-03-01 01:36:57	2009-03-01 03:20:56	1018	$0.5^{+0.3}_{-0.2}$	$1.5^{+16.7}_{-0.9}$
00030296101	54898.08683	0.58	2009-03-08 01:58:10	2009-03-08 02:11:57	825	$2.0^{+0.6}_{-0.5}$	$3.1^{+3.3}_{-0.7}$
00030296102	54902.50499	0.95	2009-03-12 12:00:25	2009-03-12 12:13:55	810	–	–
00030296103	54905.73228	0.23	2009-03-15 17:26:02	2009-03-15 17:42:55	1013	–	–
00030296104	54909.95111	0.58	2009-03-19 22:41:21	2009-03-19 22:57:49	988	–	–
00030296105	54913.22458	0.86	2009-03-23 05:11:50	2009-03-23 05:34:56	1361	–	–
00030296106	54916.97633	0.17	2009-03-26 23:17:54	2009-03-26 23:33:55	950	$1.9^{+0.5}_{-0.4}$	$3.6^{+4.7}_{-1.0}$
00030296107	54919.88405	0.42	2009-03-29 20:20:09	2009-03-29 22:05:54	1171	$1.6^{+0.5}_{-0.4}$	$2.7^{+4.6}_{-0.8}$
00030296108	54923.49186	0.72	2009-04-02 10:51:37	2009-04-02 12:44:56	1221	$1.2^{+0.4}_{-0.3}$	$2.7^{+6.5}_{-1.0}$
00030296110	54930.96239	0.35	2009-04-09 22:57:45	2009-04-09 23:13:55	970	$0.6^{+0.6}_{-0.3}$	$0.9^{+5.2}_{-0.3}$
00030296111	54933.03779	0.53	2009-04-12 00:46:55	2009-04-12 01:01:53	870	$2.2^{+0.6}_{-0.5}$	$4.2^{+5.9}_{-1.1}$
00030296112	54937.08095	0.87	2009-04-16 01:03:11	2009-04-16 02:49:57	875	–	–
00030296114	54944.31288	0.47	2009-04-23 06:35:09	2009-04-23 08:25:56	1151	$0.6^{+0.4}_{-0.2}$	$1.0^{+5.3}_{-0.3}$
00030296116	54954.85973	0.36	2009-05-03 20:31:04	2009-05-03 20:44:57	832	$3.4^{+1.0}_{-0.8}$	$5.2^{+5.6}_{-1.2}$
00030296117	54958.32941	0.65	2009-05-07 07:45:45	2009-05-07 08:02:55	1031	$0.8^{+0.7}_{-0.4}$	$0.9^{+0.7}_{-0.4}$
00030296118	54965.93235	0.29	2009-05-14 21:31:14	2009-05-14 23:13:55	782	–	–
00030296119	54968.76808	0.53	2009-05-17 18:25:08	2009-05-17 18:26:56	108	–	–
00030296120	54972.14231	0.82	2009-05-21 02:33:55	2009-05-21 04:15:56	837	–	–
00030296121	54979.70379	0.45	2009-05-28 16:01:58	2009-05-28 17:44:56	832	$6.1^{+1.7}_{-1.3}$	$9.6^{+7.8}_{-1.9}$
00030296122	54986.40167	0.02	2009-06-04 09:00:39	2009-06-04 10:22:55	70	–	–
00030296123	54992.76784	0.55	2009-06-10 14:19:26	2009-06-10 22:31:56	1086	$1.2^{+0.6}_{-0.4}$	$1.3^{+0.6}_{-0.4}$
00030296124	54993.42420	0.61	2009-06-11 09:17:45	2009-06-11 11:03:56	1176	$0.5^{+0.4}_{-0.2}$	$0.7^{+0.4}_{-0.2}$
00030296125	54996.61213	0.88	2009-06-14 12:56:59	2009-06-14 16:25:56	1354	$2.1^{+0.8}_{-0.6}$	$2.5^{+1.1}_{-0.6}$
00030296127	55004.93965	0.58	2009-06-22 21:41:14	2009-06-22 23:24:56	915	–	–
00030296128	55007.65543	0.81	2009-06-25 15:35:41	2009-06-25 15:51:57	975	$1.5^{+0.5}_{-0.4}$	$4.7^{+29.0}_{-2.3}$

Table A3. Observation log for IGR J16479−4514. Continued.

ObsID	MJD	Phase	Start time (UT) (yyyy-mm-dd hh:mm:ss)	End time (UT) (yyyy-mm-dd hh:mm:ss)	Exposure (s)	Flux[a] (erg cm^{-2} s^{-1})	Flux[b] (erg cm^{-2} s^{-1})
00030296129	55011.38840	0.12	2009-06-29 02:03:37	2009-06-29 16:34:56	419	–	–
00030296130	55014.96280	0.42	2009-07-02 22:56:55	2009-07-02 23:15:56	1141	–	–
00030296131	55018.97409	0.76	2009-07-06 23:03:26	2009-07-06 23:41:56	943	–	–
00030296132	55021.92975	0.01	2009-07-09 20:41:43	2009-07-09 23:55:56	394	–	–
00030296133	55024.35952	0.21	2009-07-12 07:45:28	2009-07-12 09:29:57	1221	$1.6^{+0.5}_{-0.3}$	$5.9^{+34.1}_{-3.1}$
00030296134	55031.75641	0.83	2009-07-19 18:04:31	2009-07-19 18:13:55	564	–	–
00030296135	55035.67416	0.16	2009-07-23 15:17:38	2009-07-23 17:03:55	702	$4.4^{+1.3}_{-1.0}$	$7.4^{+10.8}_{-1.9}$
00030296136	55038.63799	0.41	2009-07-26 13:36:27	2009-07-26 17:00:56	973	–	–
00030296137	55042.11395	0.71	2009-07-30 01:03:15	2009-07-30 04:24:55	1622	$5.5^{+1.2}_{-1.0}$	$7.1^{+2.5}_{-1.2}$
00030296138	55045.81150	0.02	2009-08-02 19:20:11	2009-08-02 19:36:56	1005	$2.1^{+0.6}_{-0.5}$	$3.5^{+3.7}_{-0.8}$
00030296139	55049.57839	0.33	2009-08-06 12:58:48	2009-08-06 14:46:56	1178	$2.3^{+0.5}_{-0.4}$	$4.2^{+4.2}_{-1.0}$
00030296141	55056.11021	0.88	2009-08-13 02:28:40	2009-08-13 02:48:44	817	$5.5^{+1.3}_{-1.1}$	$8.1^{+4.6}_{-1.5}$
00030296142	55063.74699	0.53	2009-08-20 17:46:22	2009-08-20 18:04:56	1111	$0.7^{+0.4}_{-0.2}$	$1.3^{+6.3}_{-0.5}$
00030296143	55066.49957	0.76	2009-08-23 11:50:58	2009-08-23 12:07:56	1008	–	–
00030296144	55070.24617	0.07	2009-08-27 05:46:00	2009-08-27 06:02:56	1015	$1.3^{+0.6}_{-0.4}$	$1.8^{+8.0}_{-0.5}$
00030296145	55073.25458	0.33	2009-08-30 05:52:16	2009-08-30 06:20:56	1720	$0.4^{+0.2}_{-0.1}$	$1.5^{+25.7}_{-0.9}$
00030296146	55084.63249	0.29	2009-09-10 15:02:37	2009-09-10 15:18:57	980	$0.1^{+0.3}_{-0.1}$	$0.2^{+0.7}_{-0.2}$
00030296147	55087.64497	0.54	2009-09-13 15:20:33	2009-09-13 15:36:56	983	$0.4^{+0.3}_{-0.2}$	$1.3^{+8.4}_{-0.8}$
00030296148	55091.12292	0.83	2009-09-17 02:48:03	2009-09-17 03:05:56	1073	–	–
00030296149	55094.28585	0.10	2009-09-20 06:00:18	2009-09-20 07:42:55	802	$23.6^{+4.7}_{-3.9}$	$40.8^{+38.1}_{-9.0}$
00030296150	55101.65828	0.72	2009-09-27 14:53:55	2009-09-27 16:41:56	1128	–	–
00030296151	55105.91559	0.08	2009-10-01 21:50:57	2009-10-01 22:05:57	900	$1.4^{+0.6}_{-0.4}$	$2.6^{+9.2}_{-1.0}$
00030296152	55108.11932	0.26	2009-10-04 02:43:41	2009-10-04 02:59:56	963	–	–
00030296153	55112.13932	0.60	2009-10-08 03:12:18	2009-10-08 03:28:56	998	$0.9^{+0.6}_{-0.3}$	$2.5^{+18.4}_{-1.4}$
00030296154	55122.57440	0.48	2009-10-18 13:39:20	2009-10-18 13:54:55	905	$1.4^{+0.5}_{-0.3}$	$9.0^{+79.6}_{-6.4}$
00030296155	55129.33971	0.05	2009-10-25 08:04:26	2009-10-25 08:13:55	569	$16.6^{+3.7}_{-3.0}$	$33.1^{+41.3}_{-8.8}$

Table A4. Same as Table A3 for IGR J16493−4348.

ObsID	MJD	Phase	Start time (UT) (yyyy-mm-dd hh:mm:ss)	End time (UT) (yyyy-mm-dd hh:mm:ss)	Exposure (s)	Flux (erg cm^{-2} s^{-1})	Flux (erg cm^{-2} s^{-1})
00030379003	56676.84697	0.17	2014-01-19 20:11:21	2014-01-19 20:27:54	993	$2.9^{+0.7}_{-0.5}$	$6.2^{+10.3}_{-1.9}$
00030379004	56679.12236	0.28	2014-01-22 02:49:29	2014-01-22 03:02:54	805	$1.8^{+0.9}_{-0.6}$	$13.3^{+78.5}_{-10.0}$
00030379005	56683.05763	0.48	2014-01-26 01:10:04	2014-01-26 01:35:54	1550	$3.9^{+0.7}_{-0.6}$	$5.6^{+1.6}_{-0.8}$
00030379006	56686.25279	0.64	2014-01-29 05:56:05	2014-01-29 06:11:56	950	–	–
00030379007	56690.06221	0.83	2014-02-02 01:21:14	2014-02-02 01:37:55	1000	$4.8^{+1.1}_{-0.9}$	$5.8^{+1.0}_{-0.9}$
00030379008	56693.06911	0.97	2014-02-05 01:31:07	2014-02-05 01:47:55	1008	$2.4^{+0.6}_{-0.5}$	$8.6^{+45.2}_{-4.3}$
00030379009	56697.26632	0.18	2014-02-09 06:14:06	2014-02-09 06:32:54	1128	$2.9^{+0.7}_{-0.6}$	$3.5^{+0.6}_{-0.6}$
00030379010	56704.39711	0.54	2014-02-16 01:12:45	2014-02-16 17:50:56	1221	$2.1^{+0.7}_{-0.5}$	$4.5^{+19.5}_{-1.8}$
00030379011	56707.20263	0.68	2014-02-19 04:43:41	2014-02-19 04:59:53	973	$3.3^{+0.9}_{-0.7}$	$6.0^{+9.4}_{-1.6}$
00030379012	56711.75433	0.91	2014-02-23 12:26:32	2014-02-23 23:45:55	865	$0.5^{+0.5}_{-0.3}$	$0.9^{+8.8}_{-0.4}$
00030379013	56714.47428	0.04	2014-02-26 09:44:00	2014-02-26 13:01:55	980	$3.9^{+1.3}_{-1.0}$	$5.1^{+2.6}_{-1.0}$
00030379014	56718.86194	0.26	2014-03-02 20:33:27	2014-03-02 20:48:55	925	–	–
00030379016	56725.32999	0.58	2014-03-09 07:47:26	2014-03-09 08:02:54	928	–	–
00030379017	56728.53286	0.74	2014-03-12 12:38:43	2014-03-12 12:55:54	1031	$2.3^{+0.7}_{-0.5}$	$3.4^{+2.4}_{-0.7}$
00030379018	56732.14626	0.92	2014-03-16 03:22:20	2014-03-16 03:38:53	993	$5.5^{+1.5}_{-1.3}$	$8.2^{+5.5}_{-1.9}$
00030379019	56735.61277	0.09	2014-03-19 14:33:50	2014-03-19 14:50:55	1025	$5.4^{+1.2}_{-1.0}$	$10.4^{+14.8}_{-2.9}$
00030379020	56739.61033	0.29	2014-03-23 14:35:25	2014-03-23 14:42:19	414	–	–
00030379021	56742.07266	0.42	2014-03-26 01:34:19	2014-03-26 01:54:55	1236	$1.9^{+0.5}_{-0.4}$	$2.8^{+2.0}_{-0.6}$
00030379022	56746.78347	0.65	2014-03-30 17:58:28	2014-03-30 19:37:54	953	–	–
00030379023	56749.88149	0.81	2014-04-02 21:00:45	2014-04-02 21:17:55	1031	$5.3^{+1.1}_{-0.9}$	$6.9^{+1.5}_{-1.0}$
00030379024	56753.13446	0.97	2014-04-06 00:03:17	2014-04-06 06:23:56	875	–	–
00030379025	56756.73465	0.15	2014-04-09 17:29:51	2014-04-09 17:45:54	963	$9.9^{+1.8}_{-1.5}$	$13.0^{+2.4}_{-1.7}$
00030379026	56760.79934	0.35	2014-04-13 19:03:09	2014-04-13 19:18:57	945	$3.1^{+1.0}_{-0.7}$	$6.9^{+24.6}_{-2.4}$
00030379027	56763.54492	0.49	2014-04-16 12:56:25	2014-04-16 13:12:55	990	$5.8^{+1.6}_{-1.2}$	$8.3^{+6.6}_{-1.6}$
00030379028	56767.76756	0.70	2014-04-20 17:31:39	2014-04-20 19:18:54	248	–	–
00030379029	56770.53186	0.83	2014-04-23 12:37:51	2014-04-23 12:53:54	963	$3.3^{+1.4}_{-1.0}$	$3.6^{+1.0}_{-0.8}$
00030379030	56774.74429	0.04	2014-04-27 17:43:37	2014-04-27 17:59:55	978	$2.9^{+0.8}_{-0.6}$	$6.8^{+7.2}_{-2.5}$
00030379031	56777.21166	0.17	2014-04-30 03:27:41	2014-04-30 06:41:54	1013	$3.1^{+0.8}_{-0.6}$	$4.2^{+1.4}_{-0.7}$
00030379032	56781.14707	0.36	2014-05-04 03:22:39	2014-05-04 03:40:54	1096	$1.8^{+0.6}_{-0.5}$	$2.7^{+2.7}_{-0.6}$
00030379033	56784.74352	0.54	2014-05-07 17:42:24	2014-05-07 17:58:55	990	$2.0^{+0.6}_{-0.4}$	$4.5^{+11.1}_{-1.6}$
00030379034	56788.47134	0.73	2014-05-11 11:10:33	2014-05-11 11:26:54	980	$4.7^{+1.1}_{-0.9}$	$6.5^{+2.3}_{-1.1}$
00030379035	56791.06951	0.86	2014-05-14 01:32:15	2014-05-14 01:47:55	940	$5.4^{+1.3}_{-1.0}$	$7.6^{+3.2}_{-1.3}$
00030379039	56805.67506	0.59	2014-05-28 16:03:15	2014-05-28 16:20:55	1061	$1.1^{+0.6}_{-0.4}$	$2.2^{+12.3}_{-0.9}$
00030379040	56809.80156	0.79	2014-06-01 19:05:34	2014-06-01 19:22:55	1041	$1.2^{+0.4}_{-0.3}$	$23.4^{+206.4}_{-20.3}$
00030379044	56823.45513	0.47	2014-06-15 10:47:50	2014-06-15 11:02:55	905	$1.2^{+0.6}_{-0.4}$	$1.8^{+4.2}_{-0.5}$
00030379045	56826.32881	0.61	2014-06-18 07:45:13	2014-06-18 08:01:56	993	$2.8^{+1.1}_{-0.8}$	$7.6^{+36.3}_{-3.6}$
00030379046	56830.89013	0.84	2014-06-22 04:22:40	2014-06-23 14:20:54	1186	$2.3^{+0.7}_{-0.5}$	$2.7^{+0.6}_{-0.5}$
00030379047	56833.06993	0.95	2014-06-25 01:34:30	2014-06-25 01:46:54	745	$4.4^{+1.1}_{-0.9}$	$6.8^{+4.7}_{-1.4}$
00030379048	56837.85812	0.19	2014-06-29 20:27:28	2014-06-29 20:43:54	985	$6.6^{+1.2}_{-1.0}$	$9.5^{+2.6}_{-1.3}$
00030379049	56840.40633	0.32	2014-07-02 00:03:17	2014-07-02 19:26:55	1068	$0.7^{+0.5}_{-0.3}$	$1.1^{+8.9}_{-0.5}$
00030379050	56844.53560	0.52	2014-07-06 12:45:35	2014-07-06 12:56:55	679	$3.9^{+1.6}_{-1.1}$	$4.4^{+1.4}_{-1.0}$
00030379051	56847.38144	0.66	2014-07-09 09:08:36	2014-07-09 09:09:56	80	–	–
00030379052	56851.25188	0.86	2014-07-13 05:54:29	2014-07-13 06:10:54	985	$3.8^{+0.8}_{-0.7}$	$6.2^{+4.2}_{-1.3}$
00030379053	56854.75888	0.03	2014-07-16 15:41:39	2014-07-16 20:43:55	750	–	–
00030379054	56858.59527	0.22	2014-07-20 14:08:27	2014-07-20 14:25:55	1048	$1.6^{+0.6}_{-0.4}$	$2.4^{+2.3}_{-0.5}$
00030379055	56861.72998	0.38	2014-07-23 17:27:26	2014-07-23 17:34:54	449	–	–
00030379056	56865.17643	0.55	2014-07-27 04:05:12	2014-07-27 04:22:55	1063	$3.0^{+0.8}_{-0.7}$	$3.4^{+0.7}_{-0.6}$
00030379057	56868.18760	0.70	2014-07-30 04:21:23	2014-07-30 04:38:53	1051	–	–
00030379058	56872.85217	0.93	2014-08-03 20:18:24	2014-08-03 20:35:55	1046	$6.6^{+1.6}_{-1.2}$	$12.4^{+15.2}_{-3.2}$
00030379059	56875.57199	0.07	2014-08-06 13:35:23	2014-08-06 13:51:56	993	–	–
00030379060	56879.78244	0.28	2014-08-10 18:38:31	2014-08-10 18:54:54	983	$1.1^{+0.5}_{-0.3}$	$2.9^{+22.5}_{-1.3}$
00030379061	56882.03947	0.39	2014-08-13 00:48:46	2014-08-13 01:04:54	968	–	–
00030379062	56886.64423	0.62	2014-08-17 15:24:31	2014-08-17 15:30:55	379	–	–
00030379063	56889.70647	0.77	2014-08-20 16:49:41	2014-08-20 17:04:56	915	$6.8^{+1.7}_{-1.4}$	$9.1^{+2.9}_{-1.5}$
00030379065	56896.17544	0.09	2014-08-27 04:04:38	2014-08-27 04:20:54	958	–	–
00030379066	56900.31039	0.30	2014-08-31 07:19:01	2014-08-31 07:34:53	953	$1.7^{+0.5}_{-0.4}$	$4.8^{+25.1}_{-2.1}$
00030379067	56903.50922	0.46	2014-09-03 12:04:37	2014-09-03 12:21:55	1038	$2.9^{+0.7}_{-0.6}$	$4.7^{+4.3}_{-1.0}$